Dear Olivier,
We acknowledge your carefully reading of the manuscript and the very helpful suggestions. In the following we introduce some general changes and subsequently comment on each remark.

General remarks:

In order to clarify the structure of the manuscript and to concentrate important information,

1. we introduced an new chapter “Experiment description” which now separates the “Simulation procedure” from the Results chapter.
2. We renamed the chapter “Methods: roughness data and sliding laws” to “Data”. This chapter only contains the presentation of data used in the study with a comprehensive description of the roughness data.
3. The sliding law part has moved to the “Theory”.
4. We tightened the chapter implementation.
5. Some results have been moved from the “Discussion” to “Results”.
6. We have rewritten “Introduction” and “Discussion”.

Our edits respond to the requested changes by the editor and by the reviewers. We think that the new restructur has improved the readability of the manuscript.

'Done.' denotes that this point has been solved. This could be that it has been either done directly, or that due to other changes the point does not arise any more, or that the point has been answered at another place in this text already.

Below you find a point-to-point response to all comments we received. In normal font you find the original comments, in bold our response.

Again, many thanks for all the very helpful suggestions and ideas that we received during the review process!

Best regards,

Nina and co-authors

Editor comments

[…] I think that the message is still not clear enough and that your work should be compared to other approaches (e.g. using an inversion of the basal friction).
We answer this below in the section answer to major point 1.

Moreover, the paper should emphasize much more the way the roughness parameters are estimated from the radar measurements and how the two approaches compare (how xi and xi_2 compare?).
We answer this below in the section answer to major point 2.

Major points

Answer to Major point 1: … your work should be compared to other approaches …
We have rewritten "Introduction" and "Discussion" to clarify our motivation and the differences to inversion methods.

Answer to Major Point 2: … the paper should emphasize much more the way the roughness parameters are estimated from the radar measurements and how the two approaches compare …
One key point to note is that the approach that Rippin et al. (2011) used for calculating roughness (single parameter approach, and gives the symbol xi) should be not different to the first measure of roughness covered under the two parameter approach (which is labelled as xi_2). Both of these are showing the same thing. Any subtle differences that may arise are due to different smoothing parameters or step-sizes. But in essence, they are the same thing. We think therefore, that we perhaps confuses the reviewers by referring to these as different things, and it may be better to simply refer to both as xi. The two parameter approach by Li et al. (2010) simply introduces a second parameter (eta_2 labelled in the previous versions, but perhaps better labelled as eta, which we changed now).

We have also added some more explanatory text as to how xi and eta are calculated in section 3.4 Roughness. We have not gone into huge detail, however, the information is from our perspective now sufficient but concise.

Minor remarks

- page 3, line 25 down to page 4 line 12: you seem here to tell that using the roughness approach you will be able to solve prognostic problem and have an evolving friction with time. I don't think this is completely correct: you also need to invoke a hydrology model to make the basal friction evolves with time.
In case of a 'Weertman-type' sliding law (was Eq. 14 and is now Eq. 11), the sliding velocity non-linearly depends on the basal drag (projection of the basal stress vector into the basal plane), if p>1. Thus written in the inverse form for (taub = beta^2 ub) as used in the model, the sliding parameter beta^2 is a function of the basal drag (beta^2 = beta^2(taub^(p-1), …). As the stresses inside the ice vary over time, the spatial distribution of beta^2 over time varies as well. In addition sub-melt sliding is considered that depends on the basal temperature. This quantity evolves with time, too. Thus, our approach of the basal friction does evolve with time, if one would run transient simulations.

Here we use a very simple "hydrology model" that relates the basal effective pressure to the height above buoyancy (was Eq. 15 and is now Eq. 12). The reference to Huybrechts (1992) is given in the text. The same "hydrology model" has been applied in the inverse model of Morlighem et al., 2010 (Eq. 10). As the effective pressure depends on the geometry of the ice, the basal friction would evolve with time in prognostic simulations.
We have reworked the introduction and address this in the new version.

And this is certainly the most difficult point. I guess, this could be done the same way using an inversion of beta following the procedure below:
(i) inverse for beta,
(ii) assume a friction law function of the effective pressure (e.g. Eq. (15) in Flowers et al., 2011 or your Eq. (15))
(iii) compute a water pressure distribution (assuming for example as in your approach that p_w = rho_w g (z_b-z_{sl})
(iv) compute the distribution of the friction parameters assuming the beta and p_w distribution (e.g. C_b in your Eq. (15)).

The proposed scheme would separate the hydrology component from the sliding relation. This kind of separation has been used in the study of Morlighem et al., 2010 (Eq. 10) to invert for the basal sliding parameter k^2 (similar to our beta^2, but excluding the effective pressure). One could also factor out the sub-melt sliding (or other contributions to sliding) from the sliding relation. We use the commonly used form of the sliding relation that includes a "hydrology model" as given by Huybrechts, 1992 or Bindschadler, 1983.
A sufficient complex/realistic hydrology model would be a great benefit for this and for every other ice flow model. In that case, it might be beneficial to separate the hydrology component from the sliding relation. However, this is beyond the scope of this manuscript.

You should emphasize that in comparison to the inversion procedure alone, you use some physical information on the bedrock properties to evaluate the friction law parameters, but you still require to have an hydrological model to evaluate the distribution of the basal water pressure.
It strongly depends, what is meant by 'inversion for the basal sliding'. If one would assume a sliding relation of the form tau_b = beta^2 u_b, than no additional information about bedrock properties or hydrology is required. But other forms of inversion are possible as shown by e.g. Morlighem et al., 2010, where they assumed a "hydrology model" for the inversion (see our comment above).

We state the need of physical information on the bed properties now at the end of the discussion.

- page 4, line 2: i still think that a change in the grounding line position will change the basal conditions (i.e. the water pressure distribution)
We agree, that grounding line migration would change the basal conditions. We stated in the manuscript, that changes of basal conditions due to e.g. grounding line migration could not be considered using an inversion method. This statement was not correct in general as it depends on the formulation of the inversion method, if basal hydrology (for example) is considered to be part of the inversion or not. The simple hydrology model in the inversion of Morlighem et al., 2010 could be developed further to be more realistic. This would be similar to the editor's suggestions (point (i) – (iv)) above.

We think, that subglacial erosion could be factored out of the inversion formulation similar to the hydrology.
We therefore remove the complete statement "Changes in basal conditions, by for example … not be considered with this approach".

- page 5, line 18: \mu is the effective viscosity (not ice viscosity)
Done. Also on line 13 of this page.

- below Eq. (4): is a scalar invariant -> is the second invariant
Done

- page 7, line 21: the only stress onto the ice is exerted by the water -> the only stress onto the ice is exerted by hydrostatic water pressure
Done.

- page 7, line 23: this is Eq. (11) which should then written here and only one time
Done.

- In 2.2.3 it is not clear if you account for the heat production induced by sliding (u_b . tau_b)
In equation 12 the q_fric=u_b * tau_b term is already introduced. In the text below, this term was only mentioned as "friction term". We rewrite the text:
… and the friction term induced by sliding q_fric= ….

- page 11, lines 5-11: Boundary conditions should be defined as Dirichlet, Neumann or Robin boundary conditions. It is not clear from the text what type of boundary conditions are applied here and why it is not stable.
We rewrite the section boundary condition and mention the type of the BC. Additionally the part of the implementation changes. The instabilities do not arise from the numerical scheme. As mentioned now in the text, the use of the weak constraints results in a smoother solution with less oscillations (the same applies for the implementation of the thermal boundary condition, which is now a bit more explained).

- page 15, line 29: xi should be noted xi_1.
Done. See major point 2 above.

- page 16, line 23: with N=5 (2^N=32)...
Done.

- Fig 3: the map of xi should also be added in Fig. 3 to allow the comparison with xi_2.
A figure of xi is not necessary. See major point 1 above.

- page 17, line 30: N_b is the effective pressure (not the basal normal stress which is only the ice contribution). Change at other places.
Done. Also at other places.

- Eq. (15): should be (z_b - z_{sl}) and not z_b alone
Done.

- below Eq. (15): it is speculative in both way in fact: the effective pressure can be also lower where the hydrological network has higher water pressure than rho_w g (z_b-z_sl). But I agree that for PIG this is less probable.
The term "hydrological network" was misleading in this context. The equation

for N_b does not consider any hydrological network.
Instead, the formulation of N_b implies that the base is connected to the ocean at any location in the domain that is below sea level.
We have changed the text accordingly.

- page 18, line 10: I think the expression for C_b as a function of xi should be given here.
We agree and present an equation for C_b(xi).

- page 24, line 24: what do you mean by 'exact'? I found the previous part difficult to understand and to follow.
The using of "exact" was probably misleading. We meant, the applied ranges of C_xi can be found in Wilkens (2014). We have rewritten this part in accordance with the remark above.

- page 27, line 13: cpu time constraints
Done.

- paragraph 4.3.2: I guess the analysis of the robustest of the method could be done an other way:
(i) invert for beta
(ii) knowing the roughness, T, N, obtain a map for C_L.
You would then have an information on its spatial variability.
Within our assumptions C_L is a scalar value that summarizes unknown proportionalities between the two-parameter roughness measures xi and eta and the obstacle spacing and size in Weertmans original analysis as well as the material parameters summarized in C_W.
We have used the reference simulation to calculate the spatial distribution of C_L. This information was then used the specify the range of C_L in the simulations. We now give this information together with the equation for C_L in section 4.3 "Experiment 3: Parametrisation with two-parameter roughness".

- page 28, line 13: and than increasing -> and then increasing
Done.

- page 30, line 15: large parts below the glacier are below sea level -> large parts of the bed are below sea level
Done.

- page 32, line 5: two remarks regarding the erosion: (i) at which time scale it should start to be significant? and (ii) erosion will change the bed roughness and the initially estimated roughness should then be evolved?
This is an interesting question! But we think this is beyond the scope of this paper to interpret how erosion rates would change the subglacial environment and how it could implement in the sliding law.

- Fig. 2 is not very clear and I guess not so useful.
We removed the Figure.

Manuscript prepared for The Cryosphere Discuss.
with version 2014/07/29 7.12 Copernicus papers of the LaTeX class copernicus.cls.
Date: 3 March 2015

Thermal structure and basal sliding parametrisation at Pine Island Glacier - a 3D full-Stokes model study

N. Wilkens[1,2], J. Behrens[3], T. Kleiner[2], D. Rippin[4], M. Rückamp[2], and A. Humbert[2,5]

[1]Institute for Geophysics, University of Hamburg, Germany
[2]Alfred Wegener Institute, Helmholtz Centre for Polar and Marine Research, Bremerhaven, Germany
[3]Numerical Methods in Geosciences, University of Hamburg, Germany
[4]Environment Department, University of York, Heslington, UK
[5]Department of Geosciences, University of Bremen, Germany

Correspondence to: Nina Wilkens (nina.wilkens@zmaw.de)

Abstract

Pine Island Glacier is one of the fastest changing glaciers in the Antarctic Ice Sheet and therefore in scientific focus. The glacier holds enough ice to raise global sea level significantly (~ 0.5 m), when fully melted. The question addressed by numerous modelling studies of the glacier focusses on whether the observed changes are a start for an uncontrolled and accelerating retreat. The movement of the glacier is, in the fast flowing areas, dominated by basal motion. In modelling studies the parametrisation of the basal motion is therefore crucial. Inversion methods are commonly applied to reproduce the complex surface flow structure at Pine Island Glacier, which use information of the observed surface velocity field, to constrain, among other things, basal sliding. We introduce two different approaches of combining a physical parameter, the basal roughness, with basal sliding parametrisations. This way basal sliding is connected again closer to its original formulation. We show that the basal roughness is an important and helpful parameter to consider and that many features of the flow structure can be reproduced with these approaches.

1 Introduction

In the past decades the fastest changes in ice flow velocity, ice thickness and grounding line retreat in the Antarctic Ice Sheet have been observed in the region of Pine Island Glacier (PIG), Amundsen Sea Embayment, West Antarctica ~~(Rignot, 2008; Wingham et al., 2009; Rignot,~~ Additionally, the currently observed mass loss from the Antarctic Ice Sheet is also concentrated in the area around PIG (Horwath and Dietrich, 2009; Shepherd et al., 2012). Thus PIG shows an increased contribution to global sea level rise (Mouginot et al., 2014).

The bed ~~below PIG~~ lies below sea level in large areas, making it part of a so called marine ice sheet. In combination with a retrograde bed, which slopes down from the ocean towards the center of the glacier, this setting was postulated to be intrinsically unstable, via the so called "Marine Ice Sheet Instability" hypothesis (Hughes, 1973). This hypothesis is still up

for debate (Vaughan, 2008; Gudmundsson et al., 2012), while the trigger for the changes is thought to be enhanced ocean melting of the ice shelf (Dutrieux et al., 2014).

The dynamics of PIG are crucial for its future behaviour and therefore for its contribution to sea level rise. ~~An important tool for investigating glacier dynamics are numerical ice flow models.~~ Due to the fast changes observed at PIG, a variety of modelling studies have been conducted. These studies address questions focusing on the sensitivity to changes in external conditions (ice shelf buttressing, basal conditions) (e.g. Schmeltz et al., 2002) and on the contribution to future sea level rise (e.g. Joughin et al., 2010) . The overarching question is, if the system will stabilise again in the near future, or if retreat might even accelerate (e.g. Katz and Worster, 2010; Gladstone et al., 2012; Favier et al., 2014; Seroussi et a

Ice flow models simulate the flow of glacier ice, which is due to a combination of internal deformation and basal motion. Depending on the subglacial setting, basal motion can dominate the overall motion of a glacier, which is also the case for large areas of PIG. Therefore, the basal sliding behaviour might be the crucial process to cause a further retreat or halt of the system. Gudmundsson et al. (2012) show that stable grounding line positions can be found on a retrograde bed, using models with 2 horizontal dimensions. We believe the basal sliding behaviour is a similarly important process as is the lateral buttressing.

The parametrisation of basal motion in ice flow models is therefore important for the overall dynamics of a glacier. On the other hand the difficulty of observing basal properties renders the parametrisation~~one of the most challenging parts in ice flow modelling~~. In the absence of information on basal properties like bed type, structure and availability of liquid water, control methods are applied to simulate a complex glacier flow pattern, as present at PIG ~~(e.g. MacAyeal, 1992; Joughin et al., 2009, 2010; Morlighem et al., 2010; Favier et al., 2014)~~ These methods use the measured surface velocity field to invert for basal properties or effective viscosity and to adjust basal sliding parameters. Depending on the focus of the study, these approaches can provide important insights into glacier dynamics.

~~Due to the fast changes observed at PIG, a variety of modelling studies have been conducted on it. These studies address questions focusing on the sensitivity to changes in~~

external conditions (ice shelf buttressing, basal conditions) (e.g. Schmeltz et al., 2002) and on the contribution to future sea level rise (e.g. Joughin et al., 2010) . The overarching question is, if the system will stabilise again in the near future, or if retreat might even accelerate (e.g. Katz and Worster, 2010; Gladstone et al., 2012; Favier et al., 2014; Seroussi et a

The question whether the system will stabilise again in the future is an important one to address. Nonetheless in modelling studies one needs to simplify things, being forced to focus on certain processes and neglect others. The The prognostic studies on PIG all use control methods to constrain basal sliding. Thus they define a spacially varying basal sliding parameter for the present flow state, and keep it constant during the prognostic simulations. This way the basal sliding system is somehow decoupled from the rest of the system. Changes in basal conditions, by for example subglacial erosion (Smith et al., 2012; Rippin et al., 20 dynamic hydraulic systems, can not be considered with this approach. However, the basal sliding behaviour might be the crucial process to cause a further retreat or halt of the system. Gudmundsson et al. (2012) show that stable grounding line positions can be found on a retrograde bed, using models with 2 horizontal dimensions. We believe the basal sliding behaviour is a similarly important process as is the lateral buttressing. Therefore As the observable surface velocity field is a superposition of basal motion (sliding and bed deformation) and ice deformation an inversion for basal sliding may introduce errors in the basal sliding that compensate for errors in deformational part of the ice velocity. This is especially important for the strong temperature dependence of the flow rate factor used for the ice viscosity. In addition, the spatial distribution of a basal sliding parameter represents not only the flow state at a specific time of observation, but also the assumed thermal state in the model at the same time. One could imagine an area, that has significant sliding at the time of the inversion, could freeze on at later time steps, but is allowed to slide at all times.

As the inversion for basal sliding parameters is not sufficient for the physical understanding of basal motion, we focus on basal sliding parametrisations that consider measured basal roughness distributions. This accessible bed information could be in further steps combined

with for example a sufficient realistic and time-dependent hydrological model, to consider changing basal conditions for the sliding behaviour of the glacier.

Here we present results of the thermo-mechanical 3D full-Stokes model COMice (implemented in the COMmercial finite element SOLver COMSOL Multiphysics©, cf. Pattyn et al. (2013); Wilkens (2014)), applied diagnostically to PIG. Initially we conduct a diagnostic inversion for a basal sliding parameter, as done in previous studies, to generate a reference simulation and analyse the thermal structure of the glacier. ~~Since the inversion for basal sliding parameters is not sufficient for the physical understanding of basal motion, we introduce and test in a second step~~ In subsequent experiments we introduce two methods of connecting basal roughness measures to the parametrisation of basal sliding and therefore constrain basal sliding with physically justified assumptions. Additionally, we couple the sliding behaviour to the basal temperature, adding another physically based constraint. The first method matches a single-parameter basal roughness measure for PIG, as presented in Rippin et al. (2011), onto a basal sliding parameter. The second method is based on ideas from Li et al. (2010), ~~where we use~~ with a two-parameter basal roughness measure, ~~especially calculated for this study,~~ which we apply to connect basal roughness to basal sliding. ~~The results are subsequently analysed and discussed.~~

2 The numerical flow model

2.1 Governing equations

The governing equations for the thermo-mechanical ice flow model COMice are the fluid dynamical balance equations, together with a formulation for the non-Newtonian rheology of ice. The balance equations are set up for mass, momentum and energy, and solved for the velocity vector $\boldsymbol{u}$, the pressure p and the temperature T.

The mass balance equation is given in case of incompressibility as

$$\operatorname{div} \boldsymbol{u} = 0. \tag{1}$$

The momentum balance equation is the Stokes equation, given by

$$\text{div}\,\boldsymbol{\sigma} = -\rho_{\text{i}}\boldsymbol{g}, \tag{2}$$

with the Cauchy stress tensor $\boldsymbol{\sigma}$, the density of ice ρ_{i} and the acceleration of gravity $\boldsymbol{g} = (0, 0, -g)^T$. The stress tensor $\boldsymbol{\sigma}$ is split into a velocity dependent part $\boldsymbol{\tau}$, the deviatoric stress, and a pressure dependent part $p\boldsymbol{I}$, with the identity matrix $\boldsymbol{I}$, such that $\boldsymbol{\sigma} = \boldsymbol{\tau} - p\boldsymbol{I}$. For incompressible materials only the deviatoric stress $\boldsymbol{\tau}$ can result in strains, and is thus related to the velocity field $\boldsymbol{u}$, via the strain-rate tensor $\dot{\boldsymbol{\varepsilon}}$ and the ~~ice~~ effective viscosity μ, such that $\boldsymbol{\tau} = 2\mu\dot{\boldsymbol{\varepsilon}}$. The strain-rate tensor $\dot{\boldsymbol{\varepsilon}}$ is given in components as

$$\dot{\varepsilon}_{ij} = \frac{1}{2}\left(\frac{\partial u_i}{\partial x_j} + \frac{\partial u_j}{\partial x_i}\right),$$

in relation to Cartesian basis vectors. The ~~ice~~ effective viscosity μ is described with use of Glen's flow law (Glen, 1955; Nye, 1957), such that

$$\mu(T', \dot{\varepsilon}_e) = \frac{1}{2}\left(A(T')\right)^{-1/n} \dot{\varepsilon}_e^{\frac{1-n}{n}} \quad (1-n)/n, \tag{3}$$

with the rate factor $A(T')$, the stress exponent n and the effective strain rate

$$\dot{\varepsilon}_e = \sqrt{\frac{1}{2}\text{tr}(\dot{\boldsymbol{\varepsilon}}^2)}, \tag{4}$$

which is ~~a scalar~~ the second invariant of the strain-rate tensor $\dot{\boldsymbol{\varepsilon}}$. The ~~viscosity μ depends on the~~ homologous temperature T' ~~and the effective strain rate $\dot{\varepsilon}_e$. The homologous temperature T'~~ is the temperature relative to the pressure melting point T_{pmp}, defined as

$$T' = T + \beta_c p, \tag{5}$$

with the Clausius-Clapeyron constant β_c.

The pressure melting point T_{pmp} is described for typical pressures in ice sheets ($p \lesssim 50\,\text{MPa}$) by a linear relation, such that

$$T_{\text{pmp}} = T_0 - \beta_c p, \tag{6}$$

with the melting point at low pressures T_0.

The rate factor $A(T')$ parametrises the influence of the temperature and the pressure onto the viscosity μ and is described by $A(T') = A_0 e^{-Q/RT'}$ (Greve and Blatter, 2009), with a pre-exponential constant A_0, the activation energy for creep Q and the gas constant R.

The energy balance equation is given as

$$\rho c_p(T) \left(\frac{\partial T}{\partial t} + \boldsymbol{u} \cdot \text{grad}\, T \right) = \text{div}(\kappa(T)\, \text{grad}\, T) + \psi, \tag{7}$$

with the thermal conductivity $\kappa(T)$, the specific heat capacity $c_p(T)$ and an internal heat source term $\psi = 4\mu\dot{\varepsilon}_e^2$, which connects mechanical and thermal energy.

~~The scalar values for all parameters used throughout this study are listed in Table 1.~~

2.2 Boundary conditions

The balance equations are defined under the assumption that the thermodynamic fields are sufficiently smooth, thus continuously differentiable, which is only the case for the inner parts of the glacier. The outer boundaries need specifically formulated boundary conditions. The vertical boundaries are the upper surface z_{s} and the base z_{b} of the glacier. The lateral boundaries are given by the ice divide, an inflow area and the calving front~~, indicated in Fig. 1.~~. The grounding line indicates the change of the basal boundary conditions from grounded to floating ice.

2.2.1 Mass

Since the model is applied in a diagnostic manner and therefore the geometry is fixed, only the ice base ~~z_{b}~~ needs a kinematic boundary condition, to prevent the flow to point into the

ground, and is given as ~~$\boldsymbol{u} \cdot \boldsymbol{n} = 0,$~~

$$\boldsymbol{u} \cdot \boldsymbol{n} = 0, \tag{8}$$

with the unit normal vector $\boldsymbol{n}$ pointing outwards from the surface. This ~~formulation~~ Dirichlet condition is applied to the entire ice base ~~z_b~~, including grounded and floating parts, and also implies that no basal melting is considered.

2.2.2 Stress

The upper surface ~~z_s~~ can be seen to be traction free by assuming that wind stress and atmospheric pressure are negligible compared to the typical stresses in the ice sheet, such that $\boldsymbol{\sigma} \cdot \boldsymbol{n} = 0$.

At the base of the floating ice shelf shear stress induced by circulating sea water can be neglected (Weis et al., 1999) and the only stress onto the ice is exerted by ~~the water~~ hydrostatic water pressure. As the ice shelf floats it is assumed to fulfil the floating condition and the stress applied equals the stress of the displaced water column (Greve and Blatter, 2009), such that ~~$\boldsymbol{\sigma} \cdot \boldsymbol{n} = -\rho_{\mathrm{sw}}\, g\, (z_{\mathrm{sl}} - z_{\mathrm{b}}) \cdot \boldsymbol{n}$, with the~~

$$\boldsymbol{\sigma} \cdot \boldsymbol{n} = -p_{\mathrm{sw}}\, \boldsymbol{n}, \tag{9}$$

with the water pressure p_{sw} defined as

$$p_{\mathrm{sw}} = \begin{cases} 0 & \text{for} \quad z \geq z_{\mathrm{sl}} \\ \rho_{\mathrm{sw}}\, g\, (z_{\mathrm{sl}} - z) & \text{for} \quad z < z_{\mathrm{sl}}, \end{cases} \tag{10}$$

with the density of sea water ρ_{sw} and the mean sea level z_{sl}.

For the boundary condition of the grounded ice, it is assumed that the stress vector $\boldsymbol{\sigma} \cdot \boldsymbol{n}$ is continuous across the interface, such that $\boldsymbol{\sigma} \cdot \boldsymbol{n} = \boldsymbol{\sigma}_{\mathrm{lith}} \cdot \boldsymbol{n}$, with the Cauchy stress tensor of the lithosphere $\boldsymbol{\sigma}_{\mathrm{lith}}$. Since this tensor is not known, the condition has to be approximated.

This is done with a sliding law that connects the basal sliding velocity $\boldsymbol{u}_\mathrm{b} = (\boldsymbol{u}\cdot\boldsymbol{t}_x, \boldsymbol{u}\cdot\boldsymbol{t}_y)^T$, with the unit tangential vectors $\boldsymbol{t}_x$ in the xz-plane and $\boldsymbol{t}_y$ in the yz-plane, to the basal drag $\boldsymbol{\tau}_\mathrm{b} = ((\boldsymbol{\sigma}\cdot\boldsymbol{n})\cdot\boldsymbol{t}_x, (\boldsymbol{\sigma}\cdot\boldsymbol{n})\cdot\boldsymbol{t}_y)^T$. ~~In its simplest form it can be written as a linear connection, such that~~

$$\boldsymbol{\tau}_\mathrm{b} = \beta^2 \boldsymbol{u}_\mathrm{b},$$

~~where β^2 is a basal sliding parameter including all factors~~

So called "Weertman-type sliding laws" are commonly applied in ice flow modelling studies, for which the basis was established by Weertman (1957) . He developed a mathematical description for the mechanisms that influence basal sliding. One focus lay hereby on connecting small scale processes with larger scale sliding effects. Nye (1969) and Kamb (1970) worked on related problems and they all found that the basal sliding velocity $\boldsymbol{u}_\mathrm{b}$ varies with some power of the basal shear stress $\boldsymbol{\tau}_\mathrm{b}$, depending on the dominant mechanism. Additionally they find that the basal sliding velocity $\boldsymbol{u}_\mathrm{b}$ also sensitively depends on the roughness of the bed.

The processes considered by Weertman (1957) , Nye (1969) and Kamb (1970) are only relevant for sliding over hard bedrock, where an upper limit for sliding velocities is found ($\boldsymbol{u}_\mathrm{b} < 20\,\mathrm{m\,a^{-1}}$ (Cuffey and Paterson, 2010)). For faster sliding velocities weak deformable substrate or water filled cavities have to be present. Water filled cavities reduce the contact between the ice and the bedrock, therefore effectively reducing the roughness of the bed and their effect can be considered via the effective pressure $\boldsymbol{N}_\mathrm{b} = -N_b \cdot \boldsymbol{n}$ (Bindschadler, 1983) . Fast sliding velocities can only occur when the glacier base is at pressure melting point, but also below these temperatures some sliding can be present (Fowler, 1986) . This mechanism can be reflected by a temperature function $f(T)$, which regulates sub-melt sliding. Considering the above stated thoughts leads to a sliding law of the form

$$\boldsymbol{u}_\mathrm{b} = C_\mathrm{b} |\boldsymbol{\tau}_\mathrm{b}|^{p-1} N_\mathrm{b}^{-q}\, f(T)\, \boldsymbol{\tau}_\mathrm{b} = \frac{1}{\beta^2}\boldsymbol{\tau}_\mathrm{b}, \tag{11}$$

whereby C_b is originally seen as a roughness parameter, p and q are basal sliding exponents. When written in a linearised form, all effects influencing the basal sliding ~~behaviour~~ velocity u_b, other than the linear ~~connection to basal stress. A more detailed description of sliding laws can be found in Sect. **??**, as they are of central interest for~~ relation to the basal shear stress τ_b, are summerised in a basal sliding parameter β^2.

The overburden pressure of the ice is reduced in marine parts by the uplifting water pressure (Huybrechts, 1992) , such that

$$N_b = \begin{cases} \rho_i g H & \text{for} \quad z_b \geq z_{sl} \\ \rho_i g H + \rho_{sw} g (z_b - z_{sl}) & \text{for} \quad z_b < z_{sl}, \end{cases} \tag{12}$$

with the ice thickness H. The assumptions made above imply that the base is perfectly connected to the ocean at any location in the domain that is below sea level. This assumption is plausible near the grounding line, but becomes highly speculative towards the marine regions further inland. An additional hydrological model would be needed to realistically simulate the effective basal pressure, but is beyond the scope of this study. Even though more sophisticated parametrisations for the effective pressure exist (e.g. Leguy et al. (2014)), we stick with the strong assumption stated above, as water is likely present below all fast flowing parts of PIG (Smith et al., 2013) , which coincide with the marine regions.

The temperature function $f(T)$ is taken as suggested by Budd and Jenssen (1987) as an exponential function, such that

$$f(T) = e^{\nu (T - T_{pmp})}, \tag{13}$$

with a submelt sliding parameter ν.

The dynamic boundary condition at the base is implemented consisting of a tangential part (Eq. 11) and a normal part (Eq. 12) such that

$$\boldsymbol{\sigma} \cdot \boldsymbol{n} = \beta^2 \, u_b \, \boldsymbol{t}_x + \beta^2 \, v_b \, \boldsymbol{t}_y - N_b \, \boldsymbol{n}. \tag{14}$$

This is a Robin boundary condition as it depends on the velocity and the velocity gradients.

Ice divides can be seen as mirror points where the direction of the driving stress and flow on one side of the divide opposes that of the other side. No flow across the ice divide is allowed, the tangential stresses vanish and therefore the boundary condition for ice divides is given by

$$\boldsymbol{u} \cdot \boldsymbol{n} = 0 \quad , \quad (\boldsymbol{\sigma} \cdot \boldsymbol{n}) \cdot \boldsymbol{t}_x = 0 \quad \text{and} \quad (\boldsymbol{\sigma} \cdot \boldsymbol{n}) \cdot \boldsymbol{t}_y = 0. \tag{15}$$

The boundary condition at the calving front is given by

$$\boldsymbol{\sigma} \cdot \boldsymbol{n} = -p_{\text{sw}}\, \boldsymbol{n},$$

~~with the water pressure p_{sw} defined as~~

$$p_{\text{sw}} = \begin{cases} 0 & \text{for} \quad z \geq z_{\text{sl}} \\ \rho_{\text{sw}}\, g\, (z_{\text{sl}} - z) & \text{for} \quad z < z_{\text{sl}}. \end{cases}$$

~~The boundary condition for the inflow region is given as~~ Eq. 9 and Eq. 10. For the inflow region a Dirichlet condition ~~by~~ prescribes an inflow velocity field ~~defined~~ calculated analytically with the Shallow Ice Approximation (Hutter, 1983; Morland, 1984). To the outer wall of the ice rises a no slip condition is assigned, as they are implemented as holes in the geometry.

2.2.3 Temperature

The boundary conditions for the upper surface ~~z_{s} and the ice shelf base, which is only the floating part of z_{b}, are~~ is given by Dirichlet conditions in prescribing the average annual surface temperature $T_{\text{s}}(x, y, t)$~~and the freezing temperature of seawater T_{sw}, respectively.~~ . At the base of the grounded ice ~~the~~ two cases are to be distinguished. For a cold base, that is, a basal temperature below the pressure melting point, the boundary condition has

to be formulated as a Neumann condition and the temperature gradient is prescribed as

$$\operatorname{grad} T \cdot \boldsymbol{n} = \frac{q_{\text{geo}} + q_{\text{fric}}}{\kappa(T)}, \tag{16}$$

with the geothermal ~~heat~~ flux q_{geo} and the friction heating ~~term~~ due to basal sliding $q_{\text{fric}} = \boldsymbol{u}_{\text{b}} \cdot \boldsymbol{\tau}_{\text{b}}$ (Pattyn, 2003). ~~This condition is only valid as long as $T \leq T_{\text{pmp}}$.~~ If the basal temperature ~~T~~ reaches the pressure melting point ~~T_{pmp}~~in the grounded part or the freezing temperature of seawater T_{sw} in the floating part, it has to be switched to a Dirichlet condition ~~with $T = T_{\text{pmp}}$, as the ice can not become warmer.~~

$$T = \{ \tag{17}$$

The boundary condition for the ice divide and the calving front are based on the assumption that there is no temperature gradient across the surface. It can thus be written in form of a thermal insulation $(\kappa(T) \operatorname{grad} T) \cdot \boldsymbol{n} = 0$.

~~Temperatures~~ Lastly, temperatures at the inflow boundary are prescribed by a linear profile $T_{\text{lin}} = \frac{T_{\text{pmp}} - T_{\text{s}}}{z_{\text{s}} - z_{\text{b}}}(z_{\text{s}} - z) + T_{\text{s}}$.

2.3 Implementation

The thermo-mechanically coupled 3D full-Stokes model COMice is implemented in the COMmercial finite element SOLver COMSOL Multiphysics© (cf. Wilkens (2014) for implementation details). The model has been successfully applied in the diagnostic tests in the MISMIP 3D model intercomparison project (Pattyn et al., 2013) ~~.~~

2.3.1 ~~Ice flow model~~

and the ISMIP-HOM experiments (Pattyn et al., 2008) . The ice flow model solves for the the velocity vector $\boldsymbol{u}$~~and~~ , the pressure p ~~. The~~ and the temperature T. The unstabilized Stokes equation (Eq. 2) is subject to the Babuska-Brezzi condition~~requires for numerical~~

stability, , which states that the basis functions for p are of lower order than for $\boldsymbol{u}$. Therefore we use linear elements for p and quadratic elements for $\boldsymbol{u}$ (P1+P2).

To the effective strain rate $\dot{\varepsilon}_e$ (Eq. (4)) a small value of 10^{-30}s^{-1} is added, to keep the term non-zero. Model experiments have shown, that this does not affect the overall results (Pattyn, 2003; Cornford et al., 2012) .

The boundary conditions set in the ice flow model are the kinematic and dynamic ones stated in Sect. 2.2.1 and 2.2.2, respectively. The kinematic condition at the ice base is implemented as a weak constraint, for stability reasons. Weak constraints apply boundary conditions in an integral sense and are therefore not as strict. They stand in contrast to pointwise constraints, which force the nodal value to the constraint and can thus lead to numerical instability (COMSOL, 2012) .

The basal stress vector is implemented consisting of its tangential part (Eq.(**??**)) and a normal part, given by the effective normal stress N_b (Eq. (12)), further described in Sect. **??**, such that

$$\boldsymbol{\sigma} \cdot \boldsymbol{n} = \beta^2 \, u_\mathsf{b} \, \boldsymbol{t}_x + \beta^2 \, v_\mathsf{b} \, \boldsymbol{t}_y - N_\mathsf{b} \, \boldsymbol{n},$$

with $u_b = \boldsymbol{u} \cdot \boldsymbol{t}_x$ and $v_b = \boldsymbol{u} \cdot \boldsymbol{t}_y$.

To the outer wall of the ice rises a no slip condition is assigned, as they are implemented as holes in the geometry.

2.3.1 Thermal model

The temperature is The energy balance equation Eq. 7 is discretized with linear elements, with boundary conditions from Sect. 2.2.3.

. To avoid numerical instabilities due to strong temperature advection, and thus to ensure that the element Péclet number is always < 1, we use consistent stabilization methods provided by COMSOLMultiphysics©. Equation . Eq. 7 is solved using a Galerkin Least Square (GLS) formulation (Codina, 1998) in streamline direction and crosswind diffusion (Hauke and Hughes, 1998) orthogonal to the streamline direction. The chosen stabilization

methods add less numerical diffusion the closer the numerical solution comes to the exact solution~~(COMSOL, 2012)~~ .

~~All Dirichlet conditions for the thermal model~~ To the effective strain rate $\dot{\varepsilon}_e$ (Eq. 4) a small value of 10^{-30} s^{-1} is added, to keep the term non-zero. Model experiments have shown, that this does not affect the overall results (Pattyn, 2003; Cornford et al., 2012) . The scalar values for all parameters used throughout this study are listed in Tab. 1.

All Dirichlet boundary conditions are implemented as ~~weak constraints, for stability reasons.~~

a weak constraint that means the constraint is enforced in a local average sense. This gives a smoother result than the standard method in COMSOL where constraints are enforced pointwise at node points in the mesh. The Neumann condition ~~for the~~ (Eq.16) together with the Dirichlet condition for the basal temperature at the base ~~z_b~~ (Eq. 17) is implemented in a way, that a switch between these two types is avoided. This due to the fact that a jump from T_{pmp} to T_{sw} in the area of the grounding line lead to non-convergence of the flow model. Therefore, a heat flux is prescribed, as long as $T < (T_{\text{b,max}} - 0.01)$. The expression $T_{\text{b,max}}$ prescribes a spacially variable field that defines the maximal basal temperature allowed for a region (T_{pmp} for grounded areas, T_{sw} for floating areas). If $T \geq (T_{\text{b,max}} - 0.01)$, the heat flux is gradually reduced and turns zero when $T = (T_{\text{b,max}} + 0.01)$. This procedure ensures that the basal heat flux can not increase T_{b} above $T_{\text{b,max}} + 0.01$. The smoothing of the step function ensures numerical stability, which was not found with a sharp step. The implementation is similar as in Aschwanden and Blatter (2009) .

2.3.1 Mesh

To maximise the resolution while minimising the amount of elements, we use an unstructured finite element mesh. The upper surface ~~z_s~~ is meshed first with triangles. The horizontal edge lengths are $5 - 500$ m at the grounding line and the calving front, $50 - 1000$ m at the inflow area and $100 - 2000$ m at the rest of the outer boundary. The resulting 2D surface mesh is extruded through the glacier geometry with a total of 12 vertical layers everywhere. The thickness of the vertical layers varies only with ice thickness. The spacing between the

layers is refined towards the base. The ratio of the lowest to the upper most layer thickness is 0.01, leading to a thickness of the lowest layer of about 5 m for a total ice thickness of 3000 m. The final mesh consists of $\sim 3.5 \times 10^5$ prism elements, which results in $\sim 5 \times 10^6$ degrees of freedom (DOF), when solved for all variables.

2.3.2 Solver

For solving the nonlinear system, a direct segregated solver is used, which conducts a quasi-Newton iteration. It solves consecutively: first for the velocity $\boldsymbol{u}$ and the pressure p, and thereafter for the temperature T (COMSOL, 2012). This allows for reduced working memory usage. For the remaining linear systems of equations the direct solver Pardiso (COMSOL (2012) and http://www.pardiso-project.org/, last access: 9 December 2014) is applied. While uncommon for such large numbers of DOF's, it proved to be computationally viable and robust~~, since all available iterative solvers exposed instabilities on this problem~~.

3 Data

3.1 Geometry

3.1.1 ~~Geometry and input data~~

The geometry of the model was built with a consistent set of surface elevation, ice thickness and bed topography on a 1 km grid, created by A. Le Brocq and kindly provided by her for this work. The data set represents the thickness distribution of PIG for the year 2005 and earlier. The Le Brocq data are based on the surface elevation data of Bamber et al. (2009) and the ice thickness data of Vaughan et al. (2006).

The grounding line position used is given by a combination of the positions in the MODIS Mosaic Of Antarctica (MOA, Bohlander and Scambos, 2007), corresponding to the years 2003/2004, the position in Rignot (1998), corresponding to 1996, and the position that gives the smoothest ice thickness join of the glacier geometry, assuming the floatation condition.

The model domain and grounding line is indicated in Fig. 1. The location of the ice rises pinning the ice shelf at present are detected on TerraSAR-X images from 2011, with assistance of interferograms from Rignot (2002). ~~The surface~~ Please note that ice rises are not indicated in Fig. 1.

3.2 Ice flow velocity

The observed surface velocity is taken from Rignot et al. (2011) , shown in Fig. 1, and used to validate the reference simulation. The numbering of the tributaries 1-10 feeding the central stream is based on Stenoien and Bentley (2000) . The numbering used in Vaughan et al. (2
Karlsson et al. (2009) and Rippin et al. (2011) is the same for the even numbers, but shifted by 1 for the odd numbers, as they missed tributary 1 from the numbering by Stenoien and Bentley (
We extended the numbering from Stenoien and Bentley (2000) to the tributaries 11-14, which are entering the ice shelf. Finally, Fig. 1 indicates the locations of the different types of lateral boundaries (ice divide, inflow and calving front)

3.3 Temperature

The surface temperature used here is on a 5 km grid compiled by Le Brocq et al. (2010) (ALBMAP v1), based on the temperature data described in Comiso (2000). We use the geothermal ~~heat flux q_{geo} from~~ flux q_{geo} from Purucker (2012~~(updated version of Fox Maule et al. 2~~ , updated version of Fox Maule et al. (2005)), because a variety of sensitivity tests showed, that other data sets lead to too high velocities in regions with no or little basal sliding. ~~The observed surface velocity is taken from Rignot et al. (2011) , shown in Fig. 1, and used to validate the reference simulation.~~

4 ~~Methods: roughness data and sliding laws~~

~~The central focus of this study is to investigate how basal sliding and measured basal roughness could be connected in a formulation of a basal sliding law. We will therefore~~

first describe the roughness data used throughout this study. Thereafter we will give an overview of the basal sliding laws used and elucidate their connection to basal properties.

3.1 Roughnessdata

In this study we use two different data sets measurements of basal roughness measures, compiled for the base of beneath the PIG. The first one is the a single-parameter roughness measure as presented in Rippin et al. (2011) (c.f. Fig. 4b therein) . The second one is a two-parameter roughnessmeasure calculated especially and represents the methodology often employed to define subglacial roughness (Hubbard et al., 2000; Taylor et al., 2004; Siegert e This usual approach effectively provides a measure of bed obstacle amplitude or vertical roughness. The second measure, which we calculate for this studyalong ideas from Li et al. (2010)

, follows the work of Li et al. (2010) and Wright et al. (2012) , and more recently Rippin et al. (20 introduce a second parameter which effectively provides a further measure, but this time of the frequency or wavelength of roughness obstacles (Rippin et al., 2014) . Both roughness measures are based on Fourier transformations (FT), which is a key technique to derive basal roughness. A Fast Fourier transforms (FFTs). An FT can be used to transform any surface into a sum of several periodically undulated surfaces. This way the amplitude and spatial frequency of the undulations can be expressed. For theoretical dynamic studiescharacterisi the roughness by FT works well. However, to show the spatial distribution of roughness, in a glaciological context, a In a number of recent glaciological studies, these data are transformed into a single-parameter roughness measure ($\xi$was introduced (Hubbard et al., 2000; T The single-parameter roughness measure ξ) which is defined as the integral of the spectrum within a specified wavelength interval. This method represents the amplitude of the undulations, but information about the frequency is lost. For PIG the single-parameter roughness measure ξ was calculated by Rippin et al. (2011) from a RES data set generated in austral summer 2004/05 (Vaughan et al., 2006). It is the same data set the model geometry is based on (Sect. 3), still the roughness measure includes higher resolution information,

as the derivation is based on along track sample spacing of the order of ~~30~~30 m (cf. Rippin et al. (2011)). Both data sets are then gridded with 1 km spacing.

~~Li et al. (2010) introduce a two-parameter roughness measure that represents the amplitude ξ_2 and frequency η_2~~ In applying the work of Li et al. (2010) , we introduce a second parameter so that as well as being able to represent the amplitude (ξ) we are also able to explore the frequency (η) of the undulations. ~~They introduce an interpretation how~~ This measure is calculated as the total roughness divided by the bed slope roughness (Rippin et al., 2014) . Li et al. (2010) provide guidance as to how to interpret these two parameters in terms of their different basal topographies, along with their geomorphic implications~~can be distinguished from patterns of ξ_2 and η_2~~. The interpretation from Li et al. (2010) is based on ideas by Bingham and Siegert (2009), which give an interpretation for the single-parameter roughness. Rippin et al. (2014) extended the interpretation for the two-parameter roughness measure. The implications for PIG will be discussed below.

Because of the statistical meanings of ~~ξ_2 and η_2~~ξ and η, they can be used as representatives for the vertical and horizontal length scales present at the base. To do so the integration interval for ~~$\{\xi_2,\eta_2\}$~~ $\{\xi,\eta\}$ should be in the metre-scale waveband (Li et al., 2010).

The two-parameter roughness measure for PIG was calculated for this study. The spatial resolution of the underlain data for PIG is ~~34~~34 m. A moving window is calculated with ~~($N = 5$,~~ $N = 5$ ($2^N = 32$), which is the minimum for N that should be used (e.g. Taylor et al., 2004). With a spatial resolution of ~~34~~34 m this leads to a moving window length of ~~1088~~1088 m, which is in the metre-scale waveband required by Li et al. (2010), to be able to apply the data in a sliding relation.

The received fields of ~~ξ_2 and η_2~~ ξ and η for PIG are shown in Fig.~~2.~~

2. According to Li et al. (2010), different basal properties and related geomorphic implications can be distinguished from patterns of ~~ξ_2 and η_2~~ξ and η. A marine setting with intensive deposition and fast and warm ice flow, as proposed for the central part of PIG, is characterised by low values of ~~ξ_2~~ ξ and high values of ~~η_2~~η, thus low-amplitude, low-frequency roughness.

Here it has to be noted that the second parameter ~~η_2~~ η should be more accurately seen as representing the wavelength of roughness, rather than the frequency, as high values correspond to low frequencies (Rippin et al., 2014). Nonetheless we continue here refering to ~~η_2~~ η as the roughness frequency for consistency with Li et al. (2010).

The suspected low-amplitude, low-frequency roughness is not necessarily found in the central trunk area, as can be seen in Fig. 2. Instead it seems to be more dominated by low-amplitude, high-frequency roughness, which can, following Li et al. (2010), be interpreted as a continental setting after intensive erosion, also with fast and warm ice flow. Still, this interpretation can not be seen as a contradiction to the suspicion of the presence of marine sediments. It is important to state that absolute values of roughness cannot be derived from these calculations, but rather ~~it is~~ the patterns relating to relative roughness values that are significant.

3.2 ~~Sliding laws~~

~~So called "Weertman-type sliding laws" are most commonly applied in modern modelling studies, for which the basis was established by Weertman (1957) . He developed a mathematical description for the mechanisms that influence basal sliding. One focus lay hereby on connecting small scale processes with larger scale sliding effects. Nye (1969) and Kamb (1970) worked on related problems and they all found that the basal sliding velocity u_b varies with some power of the basal shear stress τ_b, depending on the dominant mechanism. Additionally they find that the basal sliding velocity u_b also sensitively depends on the roughness of the bed.~~

4 Experiment description

~~The processes considered by Weertman (1957) , Nye (1969) and Kamb (1970) are only relevant for sliding over hard bedrock, where an upper limit for sliding velocities is found ($u_b < 20 \text{ma}^{-1}$ Cuffey and Paterson (2010)). For faster sliding velocities weak deformable substrate or water filled cavities have to be present. Water filled cavities reduce the contact~~

between the ice and the bedrock, therefore effectively reducing the roughness of the bed and their effect can be considered via the basal normal stress $\boldsymbol{N}_\mathrm{b}$, also called effective pressure (Bindschadler, 1983) .

Fast sliding velocities can only occur when the glacier base is at pressure melting point, but also below these temperatures some sliding can be present (Fowler, 1986) . This mechanism can be reflected by a temperature function $f(T)$, which regulates sub-melt sliding.

4.1 Experiment 1: Reference Simulation

Considering the above stated thoughts leads to a sliding law of the form

$$\boldsymbol{u}_\mathrm{b} = C_\mathrm{b} |\boldsymbol{\tau}_\mathrm{b}|^{p-1} N_\mathrm{b}^{-q} \; f(T) \; \boldsymbol{\tau}_\mathrm{b} = \frac{1}{\beta^2} \boldsymbol{\tau}_\mathrm{b},$$

whereby C_b is originally seen as a roughness parameter, p and q are basal sliding exponents and N_b is related to the basal normal stress, defined in Eq. (12). When written in a linearised form, as already introduced in Sect. 2.2.2, all effects influencing the basal sliding velocity $\boldsymbol{u}_\mathrm{b}$, other than the linear relation to the basal shear stress $\boldsymbol{\tau}_\mathrm{b}$, are summerized in a basal sliding parameter β^2, which leads to a spatially varying field obtained by inversion techniques.

In the following we will further define the single components in the basal sliding law, as used throughout this study.

The basal normal stress $\boldsymbol{N}_\mathrm{b}$ is a vector of the form $\boldsymbol{N}_\mathrm{b} = -N_\mathrm{b}\boldsymbol{n}$. The overburden pressure of the ice is reduced in marine parts by the uplifting water pressure (Huybrechts, 1992) , such that

$$N_\mathrm{b} = \begin{cases} \rho_\mathrm{i} g H & \text{for} \quad z_\mathrm{b} \geq z_\mathrm{sl} \\ \rho_\mathrm{i} g H + \rho_\mathrm{sw} g z_\mathrm{b} & \text{for} \quad z_\mathrm{b} < z_\mathrm{sl}, \end{cases}$$

with the ice thickness H. The assumptions made above imply a hydrology network which is perfectly connected to the ocean. This assumption is plausible near the grounding line, but becomes highly speculative towards the marine regions further inland. An additional

hydrological model would be needed to realistically simulate the effective basal pressure, but is beyond the scope of this study. Even though more soffisticated parametrisations for the effective pressure exist (e.g. Leguy et al. (2014)), we stick with the strong assumption stated above, as water is likely present below all fast flowing parts of PIG (Smith et al., 2013) , which coincide with the marine regions.

The temperature function $f(T)$ is taken as suggested by Budd and Jenssen (1987) as an exponential function, such that

$$f(T) = e^{\nu(T - T_{\mathsf{pmp}})},$$

with a submelt sliding parameter ν.

The roughness parameter C_{b} will be related to the single-parameter roughness measure from Rippin et al. (2011) in Sect. 5.2, and described in detail there.

A different approach to describe basal sliding, and also considered in this study, is introduced by Li et al. (2010) . It is based on Weertmans original formulation (Weertman, 1957) of describing the sliding mechanisms of regelation and enhanced creep, such that

$$\boldsymbol{u}_{\mathsf{b}} = C_{\mathsf{W}} \left(\boldsymbol{\tau}_{\mathsf{b}} \frac{l^2}{a^2} \right)^{\frac{(1+n)}{2}},$$

whereby C_{W} is a parameter defined by thermal and mechanical properties of the ice ($C_{\mathsf{W}} = 4.46 \times$ in our example), l is the obstacle spacing, a the obstacle size (cf. Weertman (1957)) and $n = 3$ the stress exponent.

Li et al. (2010) state that the two-parameter roughness measures ξ_2 and η_2, representing the amplitude and frequency of the roughness (cf. Sect. 3.1), can be used as a proxy for the vertical and horizontal length scales present at the base, due to their statistical meanings, such that

$$a = c_1 \, \xi_2^{\frac{1}{2}} \quad \text{and} \quad l = c_2 \, \eta_2^{\frac{1}{2}},$$

with c_1 and c_2 being proportionality factors.

Entering this into Weertmans original formulation (Eq. (22)) and additionally including a temperature function $f(T)$ as introduced above, leads to

$$u_b = C_L f(T) \left(\tau_b \frac{\eta_2}{\xi_2} \right)^{\frac{(n+1)}{2}},$$

with the constant $C_L = C_W (c_2/c_1)^{1+n}$. As the proportionality factors c_1 and c_2 are not further defined, we take C_L as a single parameter to adjust.

5 Results

We conduct numerical simulations with the model COMice set up for the PIG region. First, in Sect. 5.1, a reference simulation is conducted, where measured surface velocities are inverted for basal sliding parameters, as is commonly done for modelling the flow of PIG (e.g. Joughin et al., 2009; Morlighem et al., 2010; Favier et al., 2014; Seroussi et al., 2014) . This approach leads to a realistic surface flow structure and lets us analyse the thermal structure of the glacier. Nonetheless the approach is dissatisfying when aiming to constrain basal sliding with physical parameters at the base of the glacier. Therefore, in a second step, we introduce two approaches for the parametrisation of basal sliding that consider the basal roughness below the glacier in the formulation of a basal sliding law. The first approach, Sect. 5.2, is based on the Weertman-type sliding law as shown in Eq. (11) and considers the single-parameter roughness measure from Rippin et al. (2011) . The second approach, Sect. 5.3, is based on the idea of Li et al. (2010) to connect basal sliding to the two-parameter roughness measure, introduced in Sect. 3.1.

4.1 Reference Simulation

The main difficulty is to capture the distinct surface flow pattern, by making appropriate assumptions about the basal sliding behaviour. Many ice modelling studies use a constant

set of basal sliding parameters to reproduce somewhat realistic surface velocity fields (e.g. Rückamp, 2011; Kleiner and Humbert, 2014). This approach can not be adopted for PIG, as it leads to a shut down of parts of the fast flowing main trunk, due to very low basal shear stresses in that region (Joughin et al., 2009; Morlighem et al., 2010). Instead, for our reference simulation, an inversion for basal parameters is conducted~~, as already done by previous studies (e.g. Joughin et al., 2009; Morlighem et al., 2010; Favier et al., 2014) .~~ . This approach will lead to a realistic reproduction of the surface flow velocity field and lets us analyse the thermal structure of the glacier.

4.0.1 ~~Simulation procedure~~

The inversion method (cf. Schmeltz et al., 2002) used for our reference simulation starts by assuming ~~a linear sliding law of the form $\boldsymbol{\tau}_b = \beta^2 \boldsymbol{u}_b$ (inverted version~~ the linearized form of Eq.~~(11)),~~ 11, thus $\boldsymbol{\tau}_b = \beta^2 \boldsymbol{u}_b$, with β^2 being the basal sliding parameter to be inferred.

Additionally a simulation is conducted, where the glacier base is not allowed to slide. Therefore the resulting surface velocity field $\boldsymbol{u}_{s,nosl}$ can be seen to be solely due to internal deformation. The basal sliding velocity $\boldsymbol{u}_b$ can be approximated by subtracting the surface velocity due to internal deformation $\boldsymbol{u}_{s,nosl}$ from the measured surface velocity field $\boldsymbol{u}_{obs}$ (Rignot et al. (2011), Fig. 1). The basal drag from the simulation where no basal sliding is allowed $\boldsymbol{\tau}_{b,nosl}$ is taken as a good first representative of the real basal drag distribution $\boldsymbol{\tau}_b$. With this the field of the basal sliding parameter β^2 is defined as

$$\beta^2 = |\boldsymbol{\tau}_{b,nosl}| \left(|\boldsymbol{u}_{obs}| - |\boldsymbol{u}_{s,nosl}| \right)^{-1}, \tag{18}$$

shown in Fig.~~3.~~ 3. This is a significant different approach as in e.g. Joughin et al. (2009) , Morlighem et al. (2010) and Seroussi et al. (2014) where they minimize a cost function.

The basal sliding parameter β^2 is subsequently applied in the forward model in the linear sliding law. Since the amount of internal deformation in the ice crucially depends on the ice temperature (Eq.~~(3))~~ 3), it is important to consider a realistic temperature distribution within the ice. At this point it is important to note, that the model is applied in a diagnostic manner and therefore the received temperature distribution is a steady state one for a

fixed geometry with constant boundary conditions, which might differ from the actual transient field. Nonetheless the received field is likely to show a better approximation to reality than simply assuming a certain distribution. To consider a realistic temperature distribution within the ice, we conduct the above described procedure in an iterative manner. We first conduct a "no sliding" simulation `nosl,1`, with a constant temperature of $T = 263.15\,\mathrm{K}$. The resulting surface velocity field $\boldsymbol{u}_{\mathrm{s,nosl,1}}$ and basal drag $\boldsymbol{\tau}_{\mathrm{b,nosl,1}}$ lead to a basal sliding parameter ~~β_1^2~~β_1^2. This basal sliding parameter ~~β_1^2 enters the simulation with~~ enters a next simulation step where basal sliding `sl,1` ~~, where~~ is accounted for and the temperature field is ~~now solved for as well. The thus found~~ solved for. The temperature distribution enters the next "no sliding" simulation `nosl,2` as a constant field. ~~Now again~~ Again a basal sliding parameter ~~β_2^2~~ is found, entering the next simulation ~~with basal sliding~~ step `sl,2`, which is our final reference simulation ~~, later referred to as~~ `ref`. Thus the procedure is stopped after two iterations, and listed in a schematic manner as: `nosl,1`($T = 263.15\,\mathrm{K}$) $\rightarrow$ ~~β_1^2~~ $\beta_1^2 \rightarrow$ `sl,1`(T solved) $\rightarrow$ `nosl,2`(T from `sl,1`) $\rightarrow \beta_2^2 \rightarrow$ `sl,2/ref`(T solved).

4.0.1 ~~Velocity field~~

~~The resulting~~ The reference simulation serves as validation parameter for the subsequent experiments. As a quantitative measure the root-mean-square (RMS) deviation $\mathrm{RMS}_{\boldsymbol{u}_\mathrm{s}}$ (unit: $\mathrm{m\,a^{-1}}$) between the simulated surface velocity field ~~from the reference simulation is shown in Fig. 4, together with an indication and numbering of the different tributaries , feeding into the fast flowing central stream . The numbering of the tributaries for tributaries 1-10 is based on Stenoien and Bentley (2000) . The numbering used in Vaughan et al. (2006) , Karlsson et al. (2009) and Rippin et al. (2011) is~~ $\boldsymbol{u}_{\mathrm{s,sim}}$ and the reference surface velocity field $\boldsymbol{u}_{\mathrm{s,ref}}$ is given by

$$\mathrm{RMS}_{\boldsymbol{u}_\mathrm{s}} = \sqrt{\frac{1}{m}\sum_{i=1}^{m}(||\boldsymbol{u}_{\mathrm{s,sim}}|_i - |\boldsymbol{u}_{\mathrm{s,ref}}|_i|)^2}, \tag{19}$$

with m being the number of discrete values on a regular grid with 1 km spacing. The comparison is done in three distinct regions: fast flow velocities ("Fast"), slower flow velocities ("Slow") and the ~~same for~~ entire model region ("All") (detailed description in Wilkens (2014)). The regions of all tributaries (1-14), the ~~even numbers, but shifted by 1 for the odd numbers,~~ central stream (CS) and the shelf area (Shelf) are combined to the region "Fast", while the remainder is the region "Slow" (cf. Fig. 8b and 8c)

4.1 Experiment 2: Parametrisation with single-parameter roughness

The approach in the reference simulation is dissatisfying when aiming to constrain basal sliding with physical parameters at the base of the glacier. Therefore, we introduce in this experiment a parametrisation of basal sliding that consider the basal roughness below the glacier in the formulation of the commonly used Weertman-type sliding law (Eq. 11) with the aim to reproduce the surface velocity field of PIG. Instead of inverting for one spatially varying parameter, we now connect the basal sliding parameter C_b to the measured single-parame roughness measure ξ (Rippin et al., 2011) , Sect. 3.1, as it is closest to the originally physical meaning of C_b.

The absolute values of the roughness measure ξ are dependent on parameters chosen for its derivation (e.g. wavelength interval in Rippin et al., 2011) . At the same time the sliding parameter C_b depends not only on mechanical properties, such as basal roughness, but also thermal properties. Therefore, the roughness measure ξ can not directly be used as the sliding parameter. To use the roughness information, we select a range for the sliding parameter C_b, obtained via the approximation

$$C_\mathrm{b} = \frac{(|\boldsymbol{u}_\mathrm{obs}| - |\boldsymbol{u}_\mathrm{s,nosl}|)\, N_\mathrm{b}^q}{|\boldsymbol{\tau}_\mathrm{b,nosl}|^p}, \tag{20}$$

To obtain a roughness parameter that depends on the roughness measure ξ, the resulting range $[C_{\text{b,min}}, C_{\text{b,max}}]$ is mapped onto the range of the roughness measure $[\xi_{\text{min}}, \xi_{\text{max}}]$

$$C_{\text{b}}(\xi) = \frac{(C_{\text{b,max}} - C_{\text{b,min}}) \cdot (\xi - \xi_{\text{min}})}{(\xi_{\text{min}} - \xi_{\text{max}})} + C_{\text{b,max}}. \tag{21}$$

The lowest roughness correlates with highest basal sliding and therefore highest values of C_ξ. In the following we will refer to the basal sliding parameter $C_{\text{b}}(\xi)$, when it is related to the basal roughness measure ξ as ~~they missed tributary 1 from the numbering by Stenoien and Bentley (2000) . We extended the numbering from Stenoien and Bentley (2000) to the tributaries 11-14, which are entering the ice shelf.~~ C_ξ.

~~The~~ In total we conduct 15 simulations for experiment 2, where each parameter combination represents a potential subglacial setting. In all simulations the coefficient $p = 1$ is kept constant, while q is varied to investigate the effect of the effective pressure onto the sliding velocities ($q \in \{0, 1, 2\}$). This results in varying minimum and maximum values for C_ξ for each parameter combination. To account for potential outliers in the C_ξ distribution, we have subsequently narrowed the range of C_ξ. Hence, simulations with an identifier 1-5 are conducted with $q = 0$ and 5 different ranges of C_ξ, simulations 6-10 with $q = 1$ and 5 different ranges of C_ξ and simulations 11-15 with $q = 2$ and 5 different ranges of C_ξ. The ranges of C_ξ can be found in (Tab. 5.2 Wilkens, 2014) .

4.2 Experiment 3: Parametrisation with two-parameter roughness

The aim of this experiment is to test the idea of Li et al. (2010) for its applicability to PIG. This approach also relates the basal roughness to the basal sliding velocity but is represented by a two-parameter roughness measure for the amplitude ξ and frequency η of the undulations. The approach is based on Weertmans original formulation (Weertman, 1957) of describing

the sliding mechanisms of regelation and enhanced creep, such that

$$\boldsymbol{u}_\mathrm{b} = C_\mathrm{W} \left(\boldsymbol{\tau}_\mathrm{b} \frac{l^2}{a^2} \right)^{\frac{(1+n)}{2}}, \tag{22}$$

whereby C_W is a parameter defined by thermal and mechanical properties of the ice, l is the obstacle spacing, a the obstacle size (cf. Weertman (1957)) and $n = 3$ the stress exponent.

Li et al. (2010) state that the two-parameter roughness measures ξ and η, representing the amplitude and frequency of the roughness (cf. Sect. 3.1), can be used as a proxy for the vertical and horizontal length scales present at the base, due to their statistical meanings, such that $a = c_1\sqrt{\xi}$ and $l = c_2\sqrt{\eta}$, with c_1 and c_2 being proportionality factors.

Entering this into Weertmans original formulation (Eq. 22) and additionally including a temperature function $f(T)$ as introduced above, leads to

$$\boldsymbol{u}_\mathrm{b} = C_\mathrm{L} f(T) \left(\boldsymbol{\tau}_\mathrm{b} \frac{\eta}{\xi} \right)^{\frac{(n+1)}{2}}, \tag{23}$$

with the constant $C_\mathrm{L} = C_\mathrm{W}(c_2/c_1)^{1+n}$. As the proportionality factors c_1 and c_2 are not further defined, we take C_L as a single parameter to adjust.

To estimate an upper and lower bound for C_L the reference simulation is used to derive the spatial variability of C_L from Eq. 23 as:

$$C_\mathrm{L} = \left(|\boldsymbol{u}_\mathrm{obs}| - |\boldsymbol{u}_\mathrm{s,nosl}| \right) |\boldsymbol{\tau}_\mathrm{b,nosl}|^{-\frac{(n+1)}{2}} \left(\frac{\xi}{\eta} \right)^{\frac{(n+1)}{2}}. \tag{24}$$

The vast majority of the values lie within $C_\mathrm{L} = [3 \times 10^{-2}; 3 \times 10^{2}]$ Pa^{-2} m a^{-1}. We conduct 18 simulations for this experiment, whereby the value of C_L (Eq. 23) is varied in this range.

For all simulations conducted for experiment 3, only Eq. 2 is solved for, due to time constraints (cf. Wilkens (2014)). The temperature distribution within the ice is taken from the reference simulation. Use of the temperature field from the reference simulation gives the opportunity to connect the sliding behaviour to the basal temperature, thus only allowing ice to slide where T is close to T_{pmp}.

5 Results

5.1 Experiment 1

The resulting surface velocity field from the reference simulation is shown in Fig. 4. The general pattern of the surface velocity field is well reproduced in the reference simulation, compared to the observed surface velocity field ~~$|\boldsymbol{u}_{\text{obs}}|$ (Rignot et al., 2011, shown in Fig. 1) .~~(Fig. 1). The tributaries are all in the right location and the velocity magnitudes agree in most areas well. The highest differences between $|\boldsymbol{u}_{\text{s,ref}}|$ and $|\boldsymbol{u}_{\text{obs}}|$ are found in the ice shelf, where the simulated velocities are up to $1\,\text{km}\,\text{a}^{-1}$ smaller than the observed ones.

When solely looking at the velocity magnitudes ~~, shown in Fig. 5,~~ we again find that for higher velocities the simulated velocity field ~~$|\boldsymbol{u}_{\text{s,ref}}|$~~ is lower than the observed field ~~$|\boldsymbol{u}_{\text{obs}}|$.~~(Fig. 5). The spread around the diagonal for lower velocities appears bigger, which is mainly due to the logarithmic axes chosen. For higher flow velocities the direction of flow of the simulated field agrees well to the direction of the observed field. This is shown as a colour code for the angle offset between the velocity vectors in Fig. 5. For slower velocities the angle offset is bigger, coinciding with a higher measurement error for slower velocities.

5.1.1 ~~Temperature regime~~

~~Our simulations show~~The simulations shows, that under PIG large areas are ~~at the pressure melting point T_{pmp}. This can be seen in Fig.6, where the temperature relative to the pressure melting point at the base $T'_{\text{b,ref}}$ (homologous temperature as given in Eq. (5)), is shown~~temperate (Fig. 6). In general the overall flow pattern is reflected in the basal temperature structure,

with fast flowing areas being underlain by a temperate base. ~~This can be seen with help of the location of the tributaries in Fig.6.~~

~~Figure~~ Fig. 7 shows the homologous temperature T'_{ref} at three vertical slices, of which the location is indicated in Fig. 6. The ~~first slice shown in Fig. 7a is~~ slice located furthest away from the ice shelf ~~, towards the inner parts of the glacier. Figures 6 and 7~~ show that the base is mainly temperate, while the inner ice body ~~, (~~away from the base~~,)~~ is predominantly cold ~~. (~~Fig. 7a). A similar picture is found in the next slice ~~, shown in Fig. 7b,~~ which is located further downstream towards the ice shelf ~~. (~~Fig. 7b). Here, additionally a cold core can be seen, located in the fast flowing central stream~~(cf. Fig. 4). .~~

The next slice ~~, shown in Fig. 7c,~~ partly crosses the ice shelf ~~. (~~Fig. 7c). It can be well observed that a cold core is entering the ice shelf. ~~To the right of the ice shelf, approximately where~~ In the vicinity of tributary 11 ~~is located~~ (cf. Fig.~~6) ,~~ 1) a small temperate layer is found.

5.2 ~~Parametrisation 1: Relating the single-parameter roughness measure ξ to the basal sliding parameter C_b~~ Experiment 2

5.2.1 ~~Simulation procedure~~

~~From the results of the reference simulation, it could be suspected that different types of sliding conditions must be present below PIG. Instead of inverting for one spatially varying parameter, we now connect the basal sliding parameter C_b of Eq. (11) to the measured basal roughness ξ (Rippin et al. (2011) , Sect. 3.1), as it is closest to the originally physical meaning of C_b (cf. Sect. **??**).~~

~~In the following we will refer to the basal sliding parameter C_b, when it is related to the basal roughness measure ξ in this section as C_ξ. The absolute values of the roughness measure ξ are dependent on parameters chosen for its derivation. At the same time the sliding parameter C_b depends not only on mechanical properties, such as basal roughness, but also thermal properties. Therefore, the roughness measure ξ can not directly be used as the sliding parameter C_ξ.~~

To use the roughness information, we select a range for the sliding parameter C_b, obtained via the approximation

$$C_\mathrm{b} = \frac{(|\boldsymbol{u}_\mathrm{obs}| - |\boldsymbol{u}_\mathrm{s,nosl}|)\, N_\mathrm{b}^q}{|\boldsymbol{\tau}_\mathrm{b,nosl}|^p},$$

with the effective normal stress N_b (Eq. (12)) and $p = 1$. The basal sliding exponent q is taken as 0, 1 or 2, which regulates the effect of the effective normal stress onto the sliding velocities. The resulting logarithmic range is thereafter matched onto the normed and inverted distribution of the roughness measure ξ. It is inverted as lowest roughness correlates with highest basal sliding and therefore highest values of C_ξ. This way we make sure to derive surface velocities within a realistic range.

We conduct 15 simulations, where each parameter combination represents a potential subglacial setting. In all simulations $p = 1$, while q is varied. Simulations 1-5 are conducted with $q = 0$, simulations 6-10 with $q = 1$ and simulations 11-15 with $q = 2$. For the different values of q, the range of C_ξ is varied. The widest range of C_ξ consists of the maximum values found by approximation for C_b (Eq. (20)). Exact values can be found in (Wilkens, 2014) .

5.2.1 Velocity field

The resulting surface velocity fields are analysed in a quantitative and qualitative manner. For the quantitative manner the root-mean-square (RMS) deviation $\mathrm{RMS}_{\boldsymbol{u}_\mathrm{s}}$ between First of all we show in Fig. 8a the simulated and the reference surface velocity fields are analysed. The $\mathrm{RMS}_{\boldsymbol{u}_\mathrm{s}}$ is given by

$$\mathrm{RMS}_{\boldsymbol{u}_\mathrm{s}} = \sqrt{\frac{1}{m}\sum_{i=1}^{m}(|\boldsymbol{u}_\mathrm{s,sim}|_i - |\boldsymbol{u}_\mathrm{s,ref}|_i|)^2},$$

with m being the number of discrete values on a regular grid with 1km spacing.

The surface flow field is additionally separated into three distinct regions of fast flow velocities ("Fast"), slower flow velocities ("Slow") and the entire model region ("All") (detailed description in Wilkens (2014)). The regions of all tributaries (1-14), the central stream (CS) and the shelf area (Shelf), as shown in Fig. 8b and 8c, are combined to the region "Fast", while the remainder is the region "Slow".

Figure 8a shows the RMS$_{u_s}$ for the regions "Fast", "Slow" and "All" between the simulated and the reference surface velocity fields. deviations between the reference simulation and experiment 2 for all 15 conducted parameter combinations. It can be seen, that the "Fast" regions differ most for all parameter combinations tested here. Additionally for the entire region "All" there seems to be no single parameter combination, that minimises the RMS$_{u_s}$ valueand therefore appropriately represents the basal conditions below PIG in a sliding law. Nonetheless . Although the RMS is relatively high some of the complex surface flow features could be reproduced with our approach, which can only be seen by looking at the qualitative structure of the resulting surface flow fields. Figure 8b) Fig. 8b shows the surface velocity field of simulation 2. with $q = 0$, that means the effect of the effective pressure is cancelled out (simulation identifier 2). The location of tributary 7 and (and slightly 11) and the central stream are well reproduced.

Especially in the simulations 11-15, with Although the central stream is in general well reproduced, the inflow into the ice shelf is characterized with drop of flow velocities, which does not coincide with the observed velocities. In the simulations where the effective pressure in considered with $q = 2$ (simulation identifiers 11-15), a much better representation of the central stream and at the inflow into the ice shelf across the grounding line is found, as can be seen for example in the surface flow field from simulation 11, shown in Fig. 8c. The influence of the effective pressure N_b is thus emphasised. At the same time this method does not lead to a full reproduction of the surface flow structure. This suggests that other processes, not considered here, are may also important for the basal sliding behaviour. A possibility, not tested yet due to cpu time constraints (for a detailed description of the solution time of the simulations refer to Wilkens (2014)), is the effect of the basal stress ex-

ponent p. Increasing it would possibly to some extend regulate the high velocities in some areas, due to low basal stresses.

5.2.1 ~~Temperature regime~~

The basal homologous temperature from simulation 2 ~~, shown in Fig.9,~~ (Fig. 9) shows a very clear structure of the temperate base below the tributaries, even though they are not clearly visible in the flow field (cf. Fig. 8b). The temperature driven separation between tributaries 2 and 4 and tributaries 7 and 9 are even better visible than in the reference simulation (cf. Fig. 6). The structure of the basal homologous temperature of all other simulations look very similar to that of simulation 2, although the total area fraction of ice at pressure melting point varies, as well as the separation between the tributaries.

Another interesting feature found in the structure of the basal temperature from simulation 2 is the advection of warmer ice into the shelf. This feature can be attributed to the implementation of the thermal basal boundary condition in the shelf. While the heat flux is not allowed to raise the temperature above 271.15 K, it does not hinder the advection of warmer ice from the grounded areas.

The structure of the bands of warmer ice agree well with melt channels below the ice shelf as found by Vaughan et al. (2012).

5.3 ~~Parametrisation 2: Li-sliding~~Experiment 3

5.3.1 ~~Simulation procedure~~

~~Another approach to relate the basal roughness to the basal sliding velocity was introduced by Li et al. (2010) . We test their idea for applicability to PIG. Li et al. (2010) introduce a two-parameter roughness measure that represents the amplitude ξ_2 and frequency η_2 of the undulations, as described in Sect. 3.1.~~

~~For all simulations conducted in this section, only the ice flow model is solved for, due to time constraints (cf. Wilkens (2014)). The temperature distribution within the ice is taken from the reference simulation. The base below the fast flowing areas is thus temperate in all~~

simulations (cf. Fig. 6). Use of the temperature field from the reference simulation gives the opportunity to connect the sliding behaviour to the basal temperature, thus only allowing ice to slide where T is close to T_{pmp}. This was already done in the reference simulation (cf. Sect. 5.1) and the simulations with Parametrisation 1 (cf. Sect. 5.2). The use of the temperature function $f(T)$ slightly reduces the RMS error of the simulated surface velocity field to that of the reference simulation, but does not change the overall picture, as achieved without the use of $f(T)$.

We conduct 18 simulations, whereby the value of C_{L} (Eq. (23)) is varied in the range $[3 \times 10^{-2}; 3 \times 10^{2}]$ Pa^{-2}ma^{-1}.

5.3.1 Velocity field

The RMS$_{\boldsymbol{u}_{\text{s}}}$ deviations between the reference and simulated results are shown for all simulations in Fig. 10a, and simulation and and all conducted parameter combinations in experiment 3 show a somewhat regular pattern . (Fig. 10a). For the slower flowing areas, the RMS$_{\boldsymbol{u}_{\text{s}}}$ value increases with increasing C_{L}. For the faster flowing areas, the RMS$_{\boldsymbol{u}_{\text{s}}}$ value first slightly decreases with increasing C_{L}, and, after reaching a minimum of RMS$_{\boldsymbol{u}_{\text{s}}} = 500\,\text{m}\,\text{a}^{-1}$ for $C_{\text{L}} = 1.58\,\text{Pa}^{-2}\,\text{m}\,\text{a}^{-1}$, increases with increasing C_{L}. Since we conduct simulations with discrete values for C_{L}, the value of RMS$_{\boldsymbol{u}_{\text{s}}} = 500\,\text{m}\,\text{a}^{-1}$ represents the minimum value for the simulations conducted here, and not an absolute minimum. The RMS$_{\boldsymbol{u}_{\text{s}}}$ value for the entire region "All"“All”, shows a similar behaviour of first decreasing and than then increasing with increasing C_{L}, with a minimum RMS$_{\boldsymbol{u}_{\text{s}}}$ value of $271\,\text{m}\,\text{a}^{-1}$ for $C_{\text{L}} = 1\,\text{Pa}^{-2}\,\text{m}\,\text{a}^{-1}$.

When looking at the structure of the resulting surface flow fields, shown in Fig. 10b and 10c, it is apparent that some features of the observed surface flow field are reproduced. The central stream in all the simulations from this section is partitioned into a faster flowing upper part, and a slower flowing lower part, in the vicinity of the ice shelf.

No single value for C_{L} could be found, that reproduces the Although RMS values reveal a slight minimum, the surface velocity field of PIG is not reproduced with all its features. For higher C_{L} values, that reproduce the velocities in the central stream in a better manner, the

velocities in the slower flowing area around tributaries 3, 5, 7 and 9, located to the South of the main stream, are simulated much too high.

A striking feature of all simulations is, that the central stream is partitioned into a faster flowing upper part, and a slower flowing lower part in the vicinity of the ice shelf. We show that exemplarily for a C_L value with a low RMS value and a C_L value with a high RMS value (Fig. 10b and 10c). However, when looking at the structure of the surface flow fields it is apparent that some features of the observed surface flow field are reproduced.

Additionally, the area around tributary 14 behaves slightly different to most other tributaries. It speeds up much faster for much lower values of C_L. This is related to the low roughness measures ~~ξ_2 and η_2~~ ξ and η in that region.

6 Discussion

We have shown that the complex surface flow structure of PIG could be well reproduced with our simplified approach of an inversion for a basal sliding parameter β^2 in the reference simulation. Although the simulated flow pattern agrees well with observations, some differences in the magnitude of the surface flow velocities to observations were found. These differences are highest in the ice shelf, and might be partly related to a slower inflow from the grounded areas ~~. The simulated velocity~~ where the difference is about 1 km a^{-1} ~~slower than the observed surface velocity just before the grounding line in flow direction~~. This might be due to the position of the grounding line in our model ~~. The grounding line position in our model~~ which is further downstream than the location in 2009, to which the observed surface velocity field belongs (2007-2009). Or it might be caused by the simplified method of inferring β^2, as $\tau_{b,nosl}$ is not vanishing near the grounding line, as would be expected (~~compare to Joughin et al. (2010); Morlighem et al. (2010)~~ cf. Joughin et al. (2010) and Morlighem et al. (20

~~The~~ However, the main cause though seems to be that we did not account for the highly rifted shear margins~~in our model~~. These shear margins have been shown to be rheologically softer than undamaged ice (e.g. Humbert et al., 2009). In reality the shear margins partly uncouple the fast flowing central part from the surrounding ice. In our ~~model we treat the~~

~~shear margins~~ study we neglect the effect of shear margins and treat them rheologically equal to undamaged ice. This leads to an overestimation of the flow outside the central stream, and an underestimation within the central stream in the main trunk. The softening due to shear margins can be included in different ways, as for example done in Joughin et al. (2010); Favier et al. (2014)~~, and will be included in future model versions~~.

~~The use of our high resolution thermo-mechanical full-Stokes model COMice further allowed for an analysis of the thermal structure of the glacier. We found~~ From the simulated temperature distribution, we found that the base of the glacier ~~to be predominantly temperate , especially the fast flowing areas, while~~ is predominantly temperate with the absence of a significant temperate layer; the rest of the inner ice body is mainly cold. This finding is consistent with the general definition of an Antarctic glacier, where, due to cold conditions at the surface, the cold-temperate transition surface (CTS) (Blatter and Hutter, 1991) is located at or near the base. To form a significant basal temperate layer Blatter and Hutter (1991) ~~find~~ state that strain heating is the necessary ~~or dominant~~ mechanism. This also agrees well with our results, as the flow of PIG is dominated by basal sliding and therefore strain heating due to internal deformation is small. Only an area around tributary 11 (cf. Fig.~~6 and~~ 6 and 7c), where strain heating is much higher, shows the existence of a somewhat larger temperate layer at the base.

~~Unfortunately~~ Unfortunately there are no measured ~~temperature profiles~~ (deep) ice core temperatures available at PIG, to which our results could be compared. Nonetheless our findings of a temperate base below some parts of PIG are supported by findings from Smith et al. (2013), who find hints for the existence of water below the glacier.

As the first new parametrisation for basal sliding we tested the applicability of including actual measured roughness data in ~~a sliding law, to reproduce the surface flow field structure of PIG. As a motivation we use the original ideas that motivated the~~ the commonly used Weertman-type sliding law~~, as shown in Eq. (11), and that relate the basal sliding parameter C_b to the basal roughness ξ (Rippin et al., 2011) . We combine the spatial distribution of the basal roughness ξ with a plausible range of the basal sliding parameter C_b, to create a new basal sliding~~ . The new parameter C_ξ ~~. This new parameter C_ξ~~ is applied in the basal

sliding law ~~in different forms. On the one hand the range of values for C_ξ, on the other hand the influence of the effective pressure N_b in the sliding law is varied. The variation of the range for C_ξ is done to test the influence of the extreme values onto the flow field. The increase of the influence of the effective pressure N_b is done to investigate the importance of the marine setting, as large parts below the glacier are below sea level.~~

~~We find that the location of many tributaries can be reproduced with this approach,~~ and we were able to reproduce many of the tributaries although not the full complexity of the flow structure. ~~The~~ For instance, the central stream is in large areas underlain by a very smooth bed, indicated by a low roughness ξ, which becomes rougher towards the grounding line.

We have shown~~that, with this approach, for a fast transition across the grounding line, the~~ , that the influence of the effective ~~normal stress N_b~~ pressure onto basal sliding must be large ~~in that area. The low effective normal stress in that area leads to higher basal sliding velocities. This is especially plausible in the vicinity of the grounding line~~ , as close to the grounding line to keep the flow velocities high. As part of the overburden pressure is supported by ~~basal water or sea water~~ the basal water of the marine setting of the glacier, the effective pressure is low and basal motion is therefore facilitated.

~~At the same time the method, as applied here, does not lead to a~~ The locations of the fast flowing tributaries and the central stream are well indicated by a temperate base. The structure is visible even more clearly than for the reference simulation. This supports the idea that the location of some tributaries is influenced by basal temperatures.

A full reproduction of the surface flow structure is not achieved with the single-parameter roughness measure. This suggests that other processes, not considered here, are also important for the basal sliding behaviour. ~~A possibility not tested yet due to time constraints is the effect of the~~ In addition, the basal stress exponent p ~~. Increasing it~~ would to some extend perhaps regulate the high velocities in some areas, due to low basal stresses.

~~The locations of the fast flowing tributaries and the central stream are well indicated by a temperate base. The structure is visible even more clearly than for the reference simulation. This supports the idea that the location of some tributaries is influenced by~~

basal temperatures. The effect of p on the flow field has not been investigated here, but should be considered in the future.

For the second new parametrisation for basal sliding we test the applicability of a theory developed by Li et al. (2010) to the region of PIG, that connects a two-parameter roughness measure $\{\xi_2, \eta_2 \xi, \eta\}$ to the basal sliding law. We rewrite the equations from Li et al. (2010) , by partly using information of the original ideas from Weertman (1957) , and extend the sliding law with a temperature function $f(T)$, to apply it as a boundary condition in our flow model. We define a constant sliding parameter C_L, over which a parameter study is conducted.

This approach additionally accounts for the frequency of roughness but neglects the effective pressure. The results of the surface flow field showcertain features. The , that the central stream in all the simulations from this section experiment is partitioned into a faster flowing upper part, and a slower flowing lower part, in the vicinity of the ice shelf. No single value for C_L could be found, that reproduces the surface velocity field of PIG with all its features. For higher C_L values, that reproduce the velocities in the central stream in a better manner, the velocities in the slower flowing area around tributaries 3, 5, 7 and 9, located to the South of the main stream, are simulated much too high (cf. Fig. 10c). Additionally, the area around tributary 14 behaves slightly different to most other tributaries. It flows much faster for much lower values of C_L. This is related to the low roughness measures ξ_2 and η_2 in that region. To account for the frequency roughness does not lead to an overall better representation of the flow compared to the single-parameter approach. We expect that if the effective pressure at the base is considered in the sliding formulation of Li et al. (2010) , the results would significantly improve as the reduced effective pressure at the grounding line in the marine setting of PIG would favour higher sliding velocities.

Thus, despite Despite the inability of a complete reproduction of the surface flow field of PIG with the method presented here, it still resulted in a surface flow structure, that reveals some important methods using the roughness measure, this approach represents some important flow features, like the location of the fast flowing central stream and some of the numerous tributaries.

To derive basal properties and to adjust basal sliding parameters inversion methods use the observed velocity field and minimise the misfit between observation and model result. They require no or only very little information about the bedrock properties (e.g. bed type, temperature or availability of basal water) and result in a very good representation of the flow for the time of observation. The derived basal sliding parameters then contain not only processes related to sliding but all assumptions and approximations of the applied flow model as the surface flow is a superposition of ice deformation and basal motion. Inversion methods are therefore not sufficient to gain the knowledge about the processes at the base and their complex interplay.

In comparison to the inversion methods our approach relates sliding to the physical parameter of the subglacial bed roughness. Although the measured bed roughness is only valid for a certain period as the subglacial environment change over time, we do not expect the main features to change in the near future. One important process for prognostic simulations over longer time scales could be basal erosion (Smith et al. (2012) report relatively high erosion rates at PIG of $0.6\,\mathrm{m\,a^{-1}} \pm 0.3\,\mathrm{m\,a^{-1}}$), but this is beyond the scope of this work.

In this study the effective pressure at the base is only influenced by the height above buoyancy and effects only the areas that ground below the sea-level. This is strong restriction of the model as the sliding formulation is not connected to the very diverse hydrology at the base of the glacier. A sufficiently complex/realistic hydrology model would be a great benefit for this and for every other ice flow model. In that case, it might be beneficial to separate the hydrology component from the sliding relation. However, this is beyond the scope of this work.

7 Conclusions

The overall motion of the fast flowing parts of PIG are dominated by basal motion. The parametrisation of basal motion is therefore crucial for simulating the flow of PIG. Especially when running prognostic simulations of the glacier and aiming at analysing the sta-

bility of the system, parametrisation of basal motion is important. ~~High subglacial erosion rates are likely to change the subglacial environment over time. Also the basal temperature plays an important role in separating fast sliding regions from regions dominated by internal deformation. We introduced~~ We introduce two different approaches of connecting a basal sliding formulation to an actually measurable subglacial parameter, the basal roughness measure. Our results show, that the roughness measure is a very useful parameter to be considered for parametrisation of basal motion at PIG, as important features of the flow field could be reproduced. Nonetheless the full complexity of the problem was not captured. Our approach is a step towards a more physically based parametrisation for basal sliding, which is very important for realistic simulations of glacier dynamics.

Acknowledgements. This work was supported through the Cluster of Excellence 'CliSAP' (EXC177), University of Hamburg, funded through the German Science Foundation (DFG). We would like to thank Anne Le Brocq for providing the compiled data set for the geometry of Pine Island Glacier. We thank Stephan Cornford, an anonymous referee and the editor Olivier Gagliardini for their very helpful suggestions which improved the manuscript.

References

Aschwanden, A. and Blatter, H.: Mathematical modeling and numerical simulation of polythermal glaciers, Journal of Geophysical Research: Earth Surface, 114, F01 027, doi:10.1029/2008JF001028, 2009.

Bamber, J., Gomez-Dans, J., , and Griggs, J.: A new 1km digital elevation model of the Antarctic derived from combined satellite radar and laser data – Part 1: Data and methods, THE CRYOSPHERE, 3, 101–111, doi:10.5194/tc-3-101-2009, 2009.

Bindschadler, R.: The importance of pressurized subglacial water in separation and sliding at the glacier bed, J GLACIOL, 29, 3–19, 1983.

Bingham, R. and Siegert, M.: Quantifying subglacial bed roughness in Antarctica: implications for ice-sheet dynamics and history, QUATERNARY SCI REV, 28, 223–236, 2009.

Bingham, R. G. and Siegert, M. J.: Radar-derived bed roughness characterization of Institute and Möller ice streams, West Antarctica, and comparison with Siple Coast ice streams, Geophysical Research Letters, 34, n/a–n/a, doi:10.1029/2007GL031483, 2007.

Bingham, R. G., Siegert, M. J., Young, D. A., and Blankenship, D. D.: Organized flow from the South Pole to the Filchner-Ronne ice shelf: An assessment of balance velocities in interior East Antarctica using radio echo sounding data, Journal of Geophysical Research: Earth Surface, 112, n/a–n/a, doi:10.1029/2006JF000556, 2007.

Blatter, H. and Hutter, K.: Polythermal conditions in Arctic glaciers, J GLACIOL, 37, 261–269, 1991.

Bohlander, J. and Scambos, T.: Antarctic coastlines and grounding line derived from MODIS Mosaic of Antarctica (MOA), National Snow and Ice Data Center, Digital media, accessed 24 April 2008., Boulder, Colorado USA, 2007.

Budd, W. and Jenssen, D.: Numerical modelling of the large-scale basal water flux under the West Antarctic Ice Sheet, in: Dynamics of the West Antarctic Ice Sheet, edited by Van der Veen, C. J. and Oerlemans, J., p. 293–320, Kluwer, Dordrecht, 1987.

Codina, R.: Comparison of some finite element methods for solving the diffusion-convection-reaction equation, COMPUT METHOD APPL M, 156, 185–210, doi:10.1016/S0045-7825(97)00206-5, 1998.

Comiso, J.: Variability and Trends in Antarctic surface temperatures from in situ and satellite infrared measurements, J CLIMATE, 13, 1674–1696, 2000.

COMSOL: COMSOL Multiphysics Reference Guide, COMSOL AB, Vers. 4.3a, http://www.comsol.com/(lastaccess:10August2014), 2012.

Cornford, S., Martin, D., Graves, D., Ranken, D., Le Brocq, A., Gladstone, R., Payne, A., Ng, E., and Lipscomb, W.: Adaptive mesh, finite volume modeling of marine ice sheets, J COMPUT PHYS, 232, 529–549, 2012.

Cuffey, K. M. and Paterson, W. S. B.: The Physics of Glaciers, Butterworth-Heinemann, 4th edn., 2010.

Dutrieux, P., De Rydt, J., Jenkins, A., Holland, P., Ha, H., Lee, S., Steig, E., Ding, Q., Abrahamsen, E., and Schröder, M.: Strong sensitivity of Pine Island ice-shelf melting to climatic variability, SCIENCE, 343, 174–178, 2014.

Favier, L., Durand, G., Cornford, S., Gudmundsson, G., Gagliardini, O., Gillet-Chaulet, F., Zwinger, T., Payne, A., and Le Brocq, A.: Retreat of Pine Island Glacier controlled by marine ice-sheet instability, NATURE CLIMATE CHANGE, 4, 117–121, doi:10.1038/NCLIMATE2094, 2014.

Fowler, A.: A sliding law for glaciers of constant viscosity in the presence of subglacial cavitation, P R SOC A, 407, 147–170, 1986.

Fox Maule, C., Purucker, M., Olsen, N., and Mosegaard, K.: Heat flux anomalies in Antarctica revealed by satellite magnetic data, SCIENCE, 309, 464–467, 2005.

Gladstone, R., Lee, V., Rougier, J., Payne, A., Hellmer, H., Brocq, A. L., Shepherd, A., Edwards, T., Gregory, J., and Cornford, S.: Calibrated prediction of Pine Island Glacier retreat during the 21st and 22nd centuries with a coupled flowline model, EARTH PLANET SC LETT, 333-334, 191–199, 2012.

Glen, J.: The creep of polycrystalline ice, P R SOC A, 228, 519–538, 1955.

Greve, R. and Blatter, H.: Dynamics of Ice Sheets and Glaciers, Springer, Berlin, Heidelberg, 2009.

Gudmundsson, G., Krug, J., Durand, G., Favier, L., and Gagliardini, O.: The stability of grounding lines on retrograde slopes, THE CRYOSPHERE, 6, 1497–1505, doi:10.5194/tc-6-1497-2012, 2012.

Hauke, G. and Hughes, T. J.: A comparative study of different sets of variables for solving compressible and incompressible flows, COMPUT METHOD APPL M, 153, 1–44, doi:10.1016/S0045-7825(97)00043-1, 1998.

Helm, V., Humbert, A., and Miller, H.: Elevation and elevation change of Greenland and Antarctica derived from CryoSat-2, The Cryosphere, 8, 1539–1559, doi:10.5194/tc-8-1539-2014, 2014.

Hooke, R. L.: Principles of Glacier Mechanics, Cambridge University Press, Cambridge, 2005.

Horwath, M. and Dietrich, R.: Signal and error in mass change inferences from GRACE: the case of Antarctica, GEOPHYS J INT, 177, 849–864, 2009.

Hubbard, B., Siegert, M., and McCarroll, D.: Spectral roughness of glaciated bedrock geomorphic surfaces: implications for glacier sliding, J GEOPHYS RES, 105, 21 295–21 303, 2000.

Hughes, T.: Is the West Antarctic ice sheet disintegrating?, J GEOPHYS RES, 78, 7884–7910, 1973.

Humbert, A., Kleiner, T., Mohrholz, C., Oelke, C., Greve, R., and Lange, M.: A comparative modeling study of the Brunt Ice Shelf/Stancomb-Wills Ice Tongue system, East Antarctica, J GLACIOL, 55, 53–65, 2009.

Hutter, K.: Theoretical glaciology: Material Science of Ice and the Mechanics of Glaciers and Ice Sheets, Reidel, Tokyo, 1983.

Huybrechts, P.: The Antarctic ice sheet and environmental change: a three-dimensional modelling study, REPORTS ON POLAR RESEARCH, Alfred Wegener Institute for Polar and Marine Research, Bremerhaven, 99, 1992.

Joughin, I., Tulaczyk, S., Bamber, J., Blankenship, D., Holt, J., Scambos, T., and Vaughan, D.: Basal conditions for Pine Island and Thwaites Glaciers, West Antarctica, determined using satellite and airborne data, J GLACIOL, 55, 245–257, 2009.

Joughin, I., Smith, B., and Holland, D.: Sensitivity of 21st century sea level to ocean-induced thinning of Pine Island Glacier, Antarctica, GEOPHYS RES LETT, 37, L20 502, doi:10.1029/2010GL044819, 2010.

Kamb, B.: Sliding motion of glaciers: theory and observations, Reviews of Geophysics and Space Physics, 8, 673–728, 1970.

Karlsson, N., Rippin, D., Vaughan, D., and Corr, H.: The internal layering of Pine Island Glacier, West Antarctica, from airborne radar-sounding data, ANN GLACIOL, 50, 141–146, 2009.

Katz, R. and Worster, M.: Stability of ice-sheet grounding lines, P R SOC A, 466, 1597–1620, 2010.

Kleiner, T. and Humbert, A.: Numerical simulations of major ice streams in western Dronning Maud Land, Antarctica, under wet and dry basal conditions, J GLACIOL, 60, 215–232, 2014.

Le Brocq, A., Payne, A., and Vieli, A.: An improved Antarctic dataset for high resolution numerical ice sheet models (ALBMAP v1), EARTH SYST SCI DATA, 2, 247–260, doi:10.5194/essd-2-247-2010, 2010.

Leguy, G. R., Asay-Davis, X. S., and Lipscomb, W. H.: Parameterization of basal friction near grounding lines in a one-dimensional ice sheet model, THE CRYOSPHERE, 8, 1239–1259, doi:10.5194/tc-8-1239-2014, 2014.

Li, X., Sun, B., Siegert, M., Bingham, R., Tang, X., Zhang, D., Cui, X., and Zhang, X.: Characterization of subglacial landscapes by a two-parameter roughness index, J GLACIOL, 56, 831–836, 2010.

MacAyeal, D.: The basal stress distribution of Ice Stream E, Antarctica, inferred by control methods, J GEOPHYS RES, 97, 595–603, 1992.

Morland, L.: Thermomechanical balances of ice sheet flows, GEOPHYS ASTRO FLUID, 29, 237–266, 1984.

Morlighem, M., Rignot, E., Seroussi, H., Larour, E., Ben Dhia, H., and Aubry, D.: Spatial patterns of basal drag inferred using control methods from a full-Stokes and simpler models for Pine Island Glacier, West Antarctica, GEOPHYS RES LETT, 37, L14 502, doi:10.1029/2010GL043853, 2010.

Mouginot, J., Rignot, E., and Scheuchl, B.: Sustained increase in ice discharge from the Amundsen Sea Embayment, West Antarctica, from 1973 to 2013, GEOPHYS RES LETT, 41, 1576–1584, doi:10.1002/2013GL059069, 2014.

Nye, J.: The distribution of stress and velocity in glaciers and ice-sheets, P R SOC A, 239, 113–133, 1957.

Nye, J.: The calculation of sliding of ice over a wavy surface using Newtonian viscous approximation, P R SOC A, A311, 445–467, 1969.

Park, J., Gourmelen, N., Shepherd, A., Kim, S., Vaughan, D., and Wingham, D.: Sustained retreat of the Pine Island Glacier, GEOPHYS RES LETT, 40, 1–6, 2013.

Paterson, W.: The Physics of Glaciers, Elsevier, Oxford, 1994.

Pattyn, F.: A new three-dimensional higher-order thermomechanical ice sheet model: basic sensitivity, ice stream development, and ice flow across subglacial lakes, J GEOPHYS RES, 108, 2382, doi:10.1029/2002JB002329, 2003.

Pattyn, F., Perichon, L., Aschwanden, A., Breuer, B., de Smedt, B., Gagliardini, O., Gudmundsson, G. H., Hindmarsh, R. C. A., Hubbard, A., Johnson, J. V., Kleiner, T., Konovalov, Y., Martin, C., Payne, A. J., Pollard, D., Price, S., Rückamp, M., Saito, F., Souček, O., Sugiyama, S., and Zwinger, T.: Benchmark experiments for higher-order and full-Stokes ice sheet models (ISMIPâ€“HOM), The Cryosphere, 2, 95–108, doi:10.5194/tc-2-95-2008, 2008.

Pattyn, F., Perichon, L., Durand, G., Favier, L., Gagliardini, O., Hindmarsh, R. C., Zwinger, T., Albrecht, T., Cornford, S., Docquier, D., Fürst, J., Goldberg, D., Gudmundsson, H., Humbert, A., Hutten, M., Huybrechts, P., Jouvet, G., Kleiner, T., Larour, E., Martin, D., Morlighem, M., Payne, A., Pollard, D., Rückamp, M., Rybak, O., Seroussi, H., Thoma, M., and Wilkens, N.: Grounding-line migration in plan-view marine ice-sheet models: results of the ice2sea MISMIP3d intercomparison, J GLACIOL, 59, 2163, doi:10.3189/2013JoG12J129, 2013.

Rignot, E.: Fast recession of a West Antarctic glacier, SCIENCE, 281, 549–551, 1998.

Rignot, E.: Ice-shelf changes in Pine Island Bay, Antarctica, 1947-2000, J GLACIOL, 48, 247–256, 2002.

Rignot, E.: Changes in West Antarctic ice stream dynamics observed with ALOS PALSAR data, GEOPHYS RES LETT, 35, L12 505, doi:10.1029/2008GL033365, 2008.

Rignot, E., Mouginot, J., and Scheuchl, B.: Ice flow of the Antarctic ice sheet, SCIENCE, 333, 1427–1430, 2011.

Rippin, D., Vaughan, D., and Corr, H.: The basal roughness of Pine Island Glacier, West Antarctica, J GLACIOL, 57, 67–76, 2011.

Rippin, D., Bingham, R., Jordan, T., Wright, A., Ross, N., Corr, H., Ferraccioli, F., Brocq, A. L., Rose, K., and Siegert, M.: Basal roughness of the Institute and Moller Ice Streams, West Antarctica: Process determination and landscape interpretation, Geomorphology, 214, 139–147, doi:10.1016/j.geomorph.2014.01.021, 2014.

Rückamp, M.: Eisgeometrie und Fließdynamik der subpolaren Eiskappe von King George Island (Antarktis), Ph.D. thesis, Universität Münster, Münster, 2011.

Schmeltz, M., Rignot, E., Dupont, T., and MacAyeal, D.: Sensitivity of Pine Island Glacier, West Antarctica, to changes in ice-shelf and basal conditions: a model study, J GLACIOL, 48, 552–558, 2002.

Seroussi, H., Morlighem, M., Rignot, E., Mouginot, J., Larour, E., Schodlok, M., and Khazendar, A.: Sensitivity of the dynamics of Pine Island Glacier, West Antarctica, to climate forcing for the next 50 years, The Cryosphere, 8, 1699–1710, doi:10.5194/tc-8-1699-2014, 2014.

Shepherd, A., Ivins, E. R., A, G., Barletta, V. R., Bentley, M. J., Bettadpur, S., Briggs, K. H., Bromwich, D. H., Forsberg, R., Galin, N., Horwath, M., Jacobs, S., Joughin, I., King, M. A., Lenaerts, J. T. M., Li, J., Ligtenberg, S. R. M., Luckman, A., Luthcke, S. B., McMillan, M., Meister, R., Milne, G., Mouginot, J., Muir, A., Nicolas, J. P., Paden, J., Payne, A. J., Pritchard, H., Rignot, E., Rott, H., Sandberg Sørensen, L., Scambos, T. A., Scheuchl, B., Schrama, E. J. O., Smith, B., Sundal, A. V., van Angelen, J. H., van de Berg, W. J., van den Broeke, M. R., Vaughan, D. G., Velicogna, I., Wahr, J., Whitehouse, P. L., Wingham, D. J., Yi, D., Young, D., and Zwally, H. J.: A reconciled estimate of ice-sheet mass balance, SCIENCE, 338, 1183–1189, 2012.

Siegert, M. J., Taylor, J., Payne, A. J., and Hubbard, B.: Macro-scale bed roughness of the siple coast ice streams in West Antarctica, Earth Surface Processes and Landforms, 29, 1591–1596, doi:10.1002/esp.1100, 2004.

Siegert, M. J., Taylor, J., and Payne, A. J.: Spectral roughness of subglacial topography and implications for former ice-sheet dynamics in East Antarctica, Global and Planetary Change, 45, 249 – 263, doi:10.1016/j.gloplacha.2004.09.008, 2005.

Smith, A., Bentley, C., Bingham, R., and Jordan, T.: Rapid subglacial erosion beneath Pine Island Glacier, West Antarctica, GEOPHYS RES LETT, 39, L12 501, doi:10.1029/2012GL051651, 2012.

Smith, A., Jordan, T., Ferraccioli, F., and Bingham, R.: Influence of subglacial conditions on ice stream dynamics: Seismic and potential field data from Pine Island Glacier, West Antarctica, J GEOPHYS RES, 118, 1471–1482, 2013.

Stenoien, M. and Bentley, C.: Pine Island Glacier, Antarctica: A study of the catchment using interferometric synthetic aperture radar measurements and radar altimetry, J GEOPHYS RES, 105, 21 761–21 779, 2000.

Taylor, J., Siegert, M. J., Payne, A. J., and Hubbard, B.: Regional-scale bed roughness beneath ice masses: measurement and analysis, COMPUT GEOSCI, 30, 899–908, 2004.

Vaughan, D.: West Antarctic Ice Sheet collapse - the fall and rise of a paradigm, CLIMATIC CHANGE, 91, 65–79, 2008.

Vaughan, D., Corr, H., Ferraccioli, F., Frearson, N., O'Hare, A., Mach, D., Holt, J., Blankenship, D., Morse, D., and Young, D.: New boundary conditions for the West Antarctic ice sheet: subglacial topography beneath Pine Island Glacier, GEOPHYS RES LETT, 33, L09 501, doi:10.1029/2005GL025588, 2006.

Vaughan, D., Corr, H., Bindschadler, R., Dutrieux, P., Gudmundsson, G., Jenkins, A., Newman, T., Vornberger, P., and Wingham, D.: Subglacial melt channels and fracture in the floating part of Pine Island Glacier, Antarctica, J GEOPHYS RES, 117, F03 012, doi:10.1029/2012JF002360, 2012.

Weertman, J.: On the sliding of glaciers, J GLACIOL, 3, 33–38, 1957.

Weis, M., Greve, R., and Hutter, K.: Theory of shallow ice shelves, CONTINUUM MECH THERM, 11, 15–50, 1999.

Wilkens, N.: Pine Island Glacier - a 3D full-Stokes model study, Ph.D. thesis, Universität Hamburg, Hamburg, http://ediss.sub.uni-hamburg.de/volltexte/2014/6735/, http://ediss.sub.uni-hamburg.de/volltexte/2014/6735/(lastaccess:18August2014), 2014.

Wingham, D., Wallis, D., and Shepherd, A.: Spatial and temporal evolution of Pine Island Glacier thinning, 1995–2006, GEOPHYS RES LETT, 36, L17 501, doi:10.1029/2009GL039126, 2009.

Wright, A. P., Young, D. A., Roberts, J. L., Schroeder, D. M., Bamber, J. L., Dowdeswell, J. A., Young, N. W., Le Brocq, A. M., Warner, R. C., Payne, A. J., Blankenship, D. D., van Ommen, T. D., and Siegert, M. J.: Evidence of a hydrological connection between the ice divide and ice sheet margin in the Aurora Subglacial Basin, East Antarctica, Journal of Geophysical Research: Earth Surface, 117, n/a–n/a, doi:10.1029/2011JF002066, 2012.

Table 1. Parameter Values

Parameter	Value	Unit	Description
ρ_{i}	918	$\mathrm{kg\,m^{-3}}$	Ice density
ρ_{sw}	1028	$\mathrm{kg\,m^{-3}}$	Seawater density
g	9.81	$\mathrm{m\,s^{-2}}$	Acceleration of gravity
n	3		Stress exponent
R	8.314	$\mathrm{J\,mol^{-1}\,K^{-1}}$	Gas constant
Q	60 for $T' \leq 263.15\,\mathrm{K}$ 139 for $T' > 263.15\,\mathrm{K}$	$\mathrm{kJ\,mol^{-1}}$	Activation energy for creep (Paterson, 1994)
A_0	3.985×10^{-13} for $T' \leq 263.15\,\mathrm{K}$ 1.916×10^{3} for $T' > 263.15\,\mathrm{K}$	$\mathrm{s^{-1}\,Pa^{-3}}$	Pre-exponential constant (Paterson, 1994)
T_0	273.15	K	Melting point for low pressures
β_c	9.8×10^{-8}	$\mathrm{K\,Pa^{-1}}$	Clausius-Clapeyron constant (Hooke, 2005)
T_{sw}	271.15	K	Freezing temperature of seawater
ν	0.1		Submelt sliding parameter (Budd and Jenssen, 1987)
$\kappa(T)$	$9.828\,e^{(-5.7 \times 10^{-3}\,T\,[\mathrm{K^{-1}}])}$	$\mathrm{W\,m^{-1}\,K^{-1}}$	Thermal conductivity
$c_p(T)$	$152.5 + 7.122\,T\,[\mathrm{K^{-1}}]$	$\mathrm{J\,kg^{-1}\,K^{-1}}$	Specific heat capacity
z_{sl}	0	m	Sea level
spy	31 536 000	$\mathrm{s\,a^{-1}}$	Seconds per year

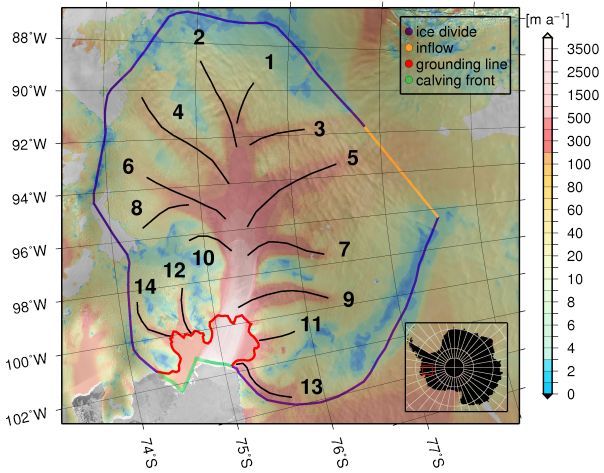

Figure 1. RADARSAT Antarctic Mapping Project (RAMP) Mosaic with the observed surface velocities from Rignot et al. (2011) and the model domain of Pine Island Glacier, with the different lateral boundaries, the grounding line and the numbered tributaries indicated.

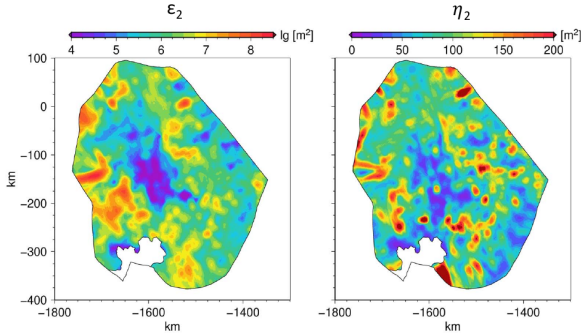

Figure 2. ~~The two-parameter~~ Calculated roughness ~~measure~~ parameters at Pine Island Glacier, given by the roughness amplitude ~~ξ_2~~ ξ and the roughness frequency ~~η_2~~ η.

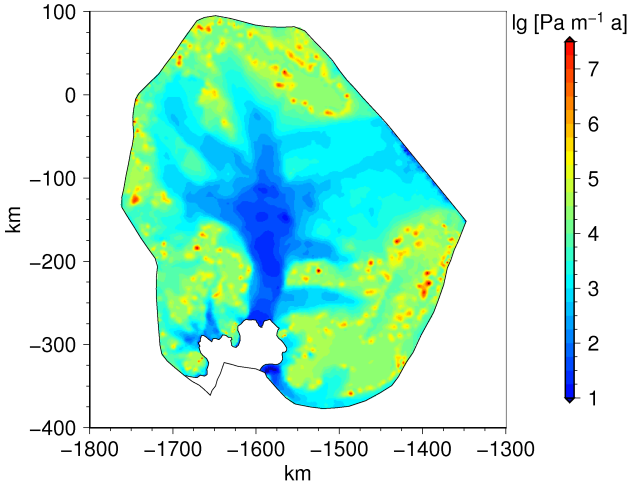

Figure 3. Spatial distribution of the basal sliding parameter β^2.

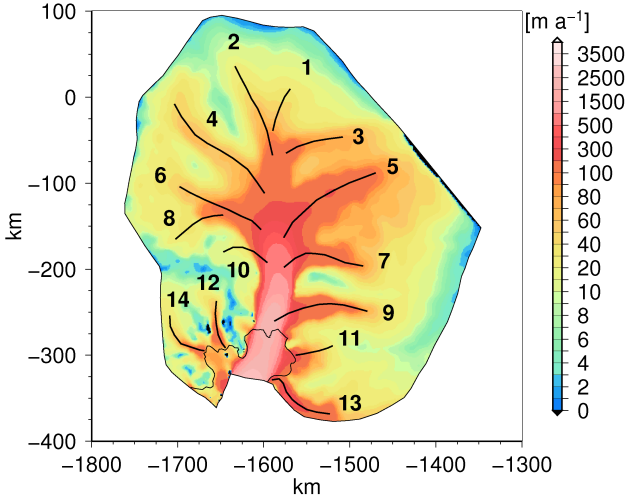

Figure 4. Surface velocity field from the reference simulation $|\boldsymbol{u}_{\mathrm{s,ref}}|$, with the numbered tributaries.

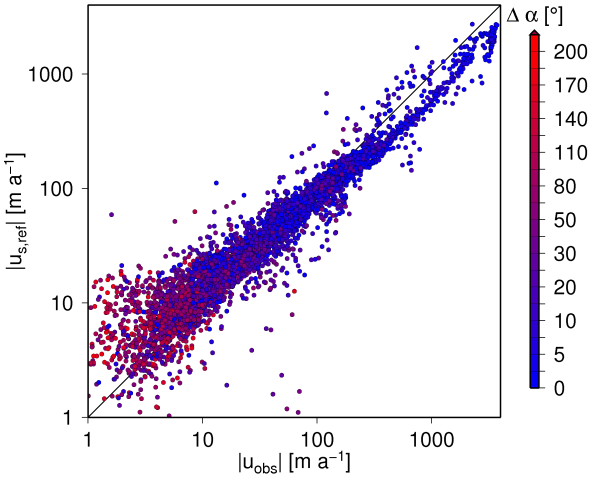

Figure 5. Observed surface velocity field $|\boldsymbol{u}_{\text{obs}}|$ vs. reference surface velocity field $|\boldsymbol{u}_{\text{s,ref}}|$. The logarithmic scales exaggerate the spread around the low speeds. The angle offset $\Delta\alpha$ between the vectors of the surface velocity field $\boldsymbol{u}_{\text{obs}}$ and the reference surface velocity field $\boldsymbol{u}_{\text{s,ref}}$ is shown as the colour code.

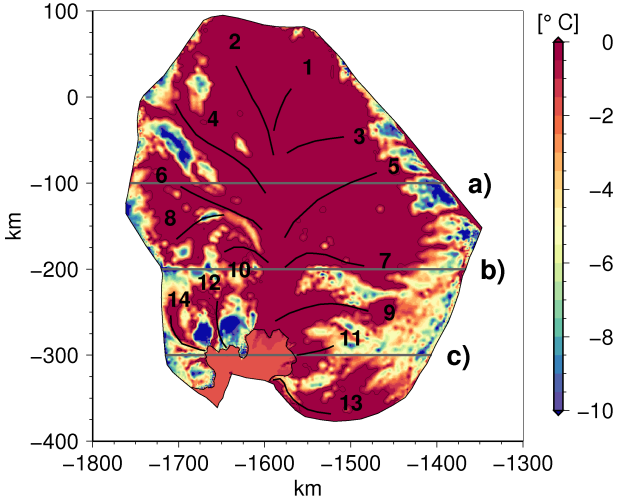

Figure 6. The basal homologous temperature from the reference simulation $T'_{\mathrm{b,ref}}$, with tributary locations in black and the location of the vertical slices a), b) and c) in Fig. 7 in grey.

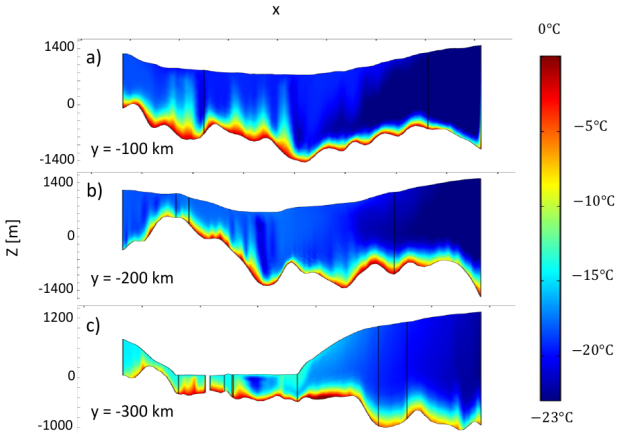

Figure 7. The internal homologous temperature from the reference simulation T'_{ref} at three vertical slices a), b) and c) (horizontal locations indicated in Fig. 6)

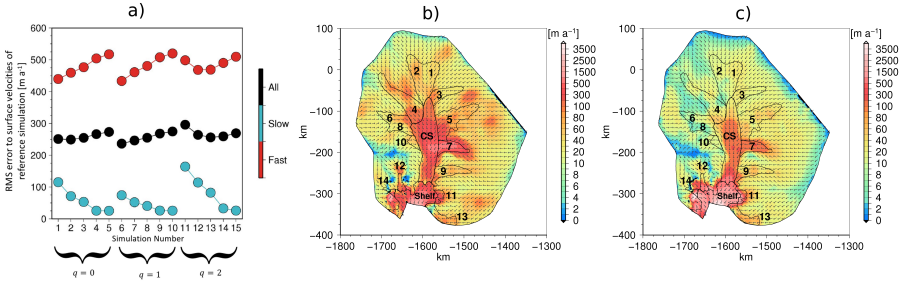

Figure 8. a) RMS error to the surface velocity field of the reference simulation versus the simulation number; b) Surface velocity field of simulation 2 with $q = 0$; c) Surface velocity field of simulation 11 with $q = 2$.

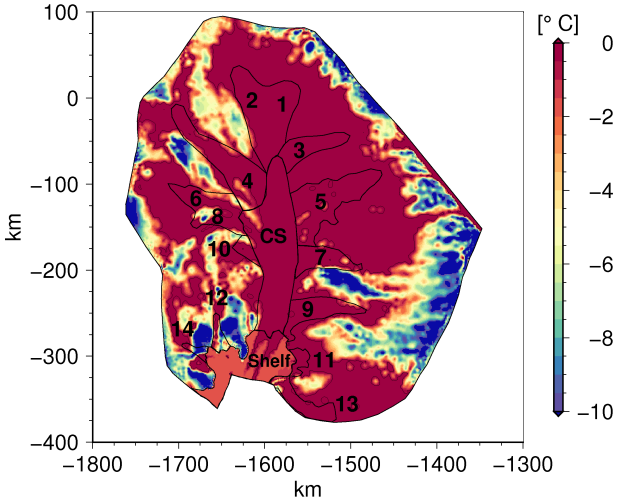

Figure 9. Basal homologous temperature of simulation 2 $T'_{\text{b,p1q0\_2}}$.

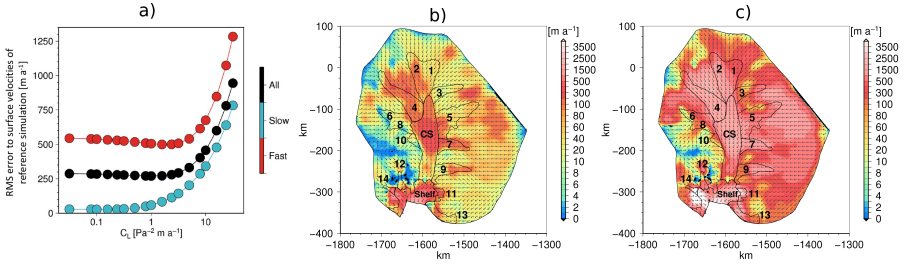

Figure 10. a) RMS error to the surface velocity field of the reference simulation versus C_L value; b) Surface velocity field with $C_\mathrm{L} = 1\,\mathrm{Pa}^{-2}\,\mathrm{m\,a}^{-1}$; c) Surface velocity field with $C_\mathrm{L} = 31.56\,\mathrm{Pa}^{-2}\,\mathrm{m\,a}^{-1}$.